ONLINE METHODS

Study cohorts. From April 2007 to April 2009, samples were obtained from 314 patients with chronic HCV (genotype 1) infection who were treated at 15 multicenter hospitals (liver units with hepatologists) throughout Japan. Each patient was treated with PEG-IFN-α2b (1.5 μg per kg body weight (μg/kg) subcutaneously once a week) or PEG-IFN-α2a (180 μg/kg once a week) plus RBV (600–1,000 mg daily depending on body weight). As a reduction in the dose of PEG-IFN-α and RBV can contribute to a less sustained virological response[21], only patients with an adherence of >80% dose for both drugs during the first 12 weeks were included in this study. HBsAg-positive and/or anti-HIV–positive individuals were excluded from this study.

NVR (seen in ~20% of total treated patients) was defined as less than a 2-log-unit decline in the serum level of HCV RNA from the pre-treatment baseline value within the first 12 weeks and detectable viremia 24 weeks after treatment. VR was defined as the achievement of SVR or transient TVR in this study; SVR was defined as undetectable HCV RNA in serum 6 months after the end of treatment, whereas TVR was defined as a reappearance of HCV RNA in serum after treatment was discontinued in a patient who had undetectable HCV RNA during the therapy or on completion of the therapy. Of 878 patients with HCV genotype 1 treated by PEG-IFN-α/RBV at 14 hospitals, only 114 (13.0%) met the criteria for NVR in this study. For the GWAS stage of the study, a case-control study was conducted comparing individuals with NVR (82 individuals) and VR (72 individuals). For the replication stage, an independent cohort of samples from 172 Japanese patients with HCV genotype 1, including 50 with NVR and 122 with VR, was obtained from an independent cohort study at Tokyo Medical and Dental University Hospital (Ochanomizu Liver Conference Study Group) and Musashino Red Cross Hospital. Clinical data from the combined cohorts, with a total of 140 SVR, 46 TVR and 128 NVR patients, are shown in **Supplementary Table 4.**

Informed consent was obtained from each patient who participated in the study. The study protocol conforms to the relevant ethical guidelines as reflected in *a priori* approval by the ethics committees of all the participating universities and hospitals.

SNP genotyping and data cleaning. In the GWAS stage, we genotyped 154 Japanese patients with HCV receiving PEG-IFN-α/RBV treatment using the Affymetrix Genome-Wide Human SNP Array 6.0 according to the manufacturer's instructions. After exclusion of 4 NVR samples and 8 SVR samples with QC call rates <95%, the remaining 142 samples were recalled using the Birdseed version 3 software (Affymetrix). The average overall call rate of 78 NVR and 64 VR samples reached 99.46% and 99.46%, respectively. We then applied the following thresholds for QC in data cleaning: SNP call rate ≥95% for all samples, MAF ≥1% for all samples and HWE P value ≥0.001 for VR group[22,23]. A total of 621,220 SNPs on autosomal chromosomes passed the QC filters and were used for association analysis. All cluster plots for the SNPs showing $P < 0.001$ in association analyses by comparing allele frequencies in NVR and VR groups were checked by visual inspection. SNPs with ambiguous genotype calls were excluded. **Supplementary Table 5** shows SNPs that might be weakly associated with NVR ($P < 10^{-4}$).

Although the 12 samples noted above were excluded from the GWAS stage by data cleaning, their quality was good enough for the SNP typing in the replication study, and thus they were included in the replication stage. In the subsequent replication stage with high-density association mapping, SNP genotyping in the independent set of 172 patients was completed using the DigiTag2 assay[24] and direct sequencing using the Applied Biosystems 3730 DNA Analyzer (Applied Biosystems). In addition, strongly associated SNPs identified in the GWAS stage were also genotyped for the GWAS samples using the DigiTag2 assay, and the results were 100% concordant to those from the GWAS platform.

Screening for new polymorphisms. To determine possible genomic variants in the region of *IL28B* and its promoter, we sequenced the 3.3-kb region in a total of 48 Japanese patients with HCV (28 NVR and 20 VR). We selected 7 samples from NVR patients who were minor allele homozygotes for 2 SNPs (rs12980275 and rs8099917), 11 samples from NVR and 10 samples from VR heterozygotes, and 10 samples from NVR and 10 samples from VR major allele homozygotes. The sequencing primers were designed using the Visual OMP Nucleic Acid software (**Supplementary Table 6**). PCR was carried using TaKaRa LA *Taq* polymerase (Takara Biochemicals) under the following thermal cycler conditions: stage 1, 94 °C for 1 min; stage 2, 98 °C for 10 s, 68 °C for 15 min, for a total of 30 cycles; stage 3, 72 °C for 10 min. A 50-μl PCR analysis was performed using 2.5 U TaKaRa LA *Taq* with 1× LA PCR buffer II, 0.4 mM dNTP, 10 pmol of each primer and 10 ng of genomic DNA. For sequencing, 7.0 μl of the PCR products were incubated with 3 μl of Exonuclease I/Shrimp Alkali Phosphatase (Takara Biochemicals) first for 90 min at 37 °C and then for another 10 min at 80 °C. Sequencing reactions were performed with the use of a BigDye Terminator Cycle Sequencing FS Ready Reaction Kit (Applied Biosystems). After purification with MultiScreen-HV (Millipore) and Sephadex G-50 Fine (GE Healthcare UK Ltd.), the reaction products were applied to the Applied Biosystems 3730 DNA Analyzer.

In the variation screening, three SNPs (rs8103142, rs28416813 and rs4803219) and a few infrequent variations were detected. We then typed these SNPs in all of the 314 patients.

Statistical analysis. The observed association between a SNP and response to PEG-IFN-α/RBV treatment was assessed by χ^2 test with a two-by-two contingency table in three genetic models: allele frequency model, dominant-effect model and recessive-effect model. SNPs on the X chromosome were removed because gender was not matched between the NVR group and the VR group. A total of 621,220 SNPs passed the QC filters in the GWAS stage; therefore, significance levels after the Bonferroni correction for multiple testing were $P = 8.05 \times 10^{-8}$ (0.05/621,220) in the GWAS stage and $P = 0.0031$(0.05/16) in the replication stage. None of the 16 markers genotyped in the replication stage showed deviations from Hardy-Weinberg equilibrium in the VR group ($P > 0.05$).

The inflation factor λ was estimated based on the median χ^2 and revealed to be 1.029 (median) and 1.011 (mean), suggesting that the population substructure should not have any substantial effect on the statistical analysis (**Supplementary Fig. 1**). In addition, the principal component analysis on the 142 patients (78 NVR samples and 64 VR samples) analyzed in the GWAS stage together with the HapMap samples also revealed that the effect of population stratification was negligible (**Supplementary Fig. 2**).

For the replication study and the high-density association mapping, 16 SNPs were selected from the region of ~40 kb (chr. 9, nucleotide positions 44421319–44461718; build 35) containing the significantly associated SNPs (rs12980275 and rs8099917) in the GWAS stage by analyzing, using Haploview software, LD and haplotype structure based on the HapMap data for individuals of Japanese descent. These SNPs included tagging SNPs estimated on the basis of haplotype blocks, SNPs located within the *IL28B* and *IL28A* genes (rs11881222 and rs576832, respectively) and the significantly associated SNPs identified in the GWAS stage (**Supplementary Table 1**). On the basis of the genotype data from the total of 314 patients in the GWAS stage and replication stages, haplotype blocks were estimated using the four-gamete rule, and three blocks were observed (**Fig. 2**). Association of haplotype with response to PEG-IFN-α/RBV treatment was analyzed using Haploview software.

The logistic regression model was used to assess the factors associated with NVR. STATA 10 (Statacorp LP) was used for all analysis. Age, platelet count, and aminotransferase (ALT) and HCV-RNA levels were applied as continuous variables.

Real-time quantitative RT-PCR for *IL28* gene. A layer of mononuclear cells was collected via Ficoll from peripheral blood. Total RNA was isolated using the RNeasy Mini Kit and the RNase-Free DNase Set (Qiagen) according to the manufacturer's protocol. First-strand cDNA was synthesized using SuperScript II reverse transcriptase with Oligo $(dT)_{12-18}$ primer (Invitrogen). The relative quantification of the target gene was determined using Custom TaqMan Gene Expression Assays, and the expression of glyceraldehyde-3-phosphate dehydrogenase was used to normalize the gene expression level (Applied Biosystems) according to the manufacturer's protocol. The data were analyzed by the $2[-\Delta\Delta C_t]$ method using Sequence Detector version 1.7 software (Applied Biosystems). A standard curve was prepared by serial tenfold dilutions of

© 2009 Nature America, Inc. All rights reserved.

human cDNA. The curve was linear over 7 logs with a correlation coefficient of 0.998. The specific detection of *IL28B* in real-time PCR is hard to establish, because the nucleotide differences between *IL28A* and *IL28B* consist of only 9 nucleotides scattered throughout the gene. Primers and probes are designed for the *IL28* gene (**Supplementary Table 6**).

URLs. The results of the present GWAS have been registered at a public database: https://gwas.lifesciencedb.jp/cgi-bin/gwasdb/gwas_top.cgi.

21. McHutchison, J.G. *et al.* Adherence to combination therapy enhances sustained response in genotype-1-infected patients with chronic hepatitis C. *Gastroenterology* **123**, 1061–1069 (2002).
22. Miyagawa, T. *et al.* Variant between *CPT1B* and *CHKB* associated with susceptibility to narcolepsy. *Nat. Genet.* **40**, 1324–1328 (2008).
23. Miyagawa, T. *et al.* Appropriate data cleaning methods for genome-wide association study. *J. Hum. Genet.* **53**, 886–893 (2008).
24. Nishida, N., Tanabe, T., Takasu, M., Suyama, A. & Tokunaga, K. Interferons alpha and lambda inhibit hepatitis C virus replication with distinct signal transduction and gene regulation kinetics. *Gastroenterology* **131**, 1887–1898 (2006).

© 2009 Nature America, Inc. All rights reserved.

The American Journal of Pathology, Vol. 175, No. 2, August 2009
Copyright © American Society for Investigative Pathology
DOI: 10.2353/ajpath.2009.081061

Gastrointestinal, Hepatobiliary and Pancreatic Pathology

Endothelial to Mesenchymal Transition via Transforming Growth Factor-β1/Smad Activation Is Associated with Portal Venous Stenosis in Idiopathic Portal Hypertension

Azusa Kitao,*† Yasunori Sato,* Seiko Sawada-Kitamura,* Kenichi Harada,* Motoko Sasaki,* Hiroyasu Morikawa,‡ Susumu Shiomi,§ Masao Honda,¶ Osamu Matsui,† and Yasuni Nakanuma*

From the Departments of Human Pathology, Radiology,† and Gastroenterology,¶ Kanazawa University Graduate School of Medicine, Kanazawa; and the Departments of Hepatology,‡ and Nuclear Medicine,§ Osaka City University Graduate School of Medicine, Osaka, Japan*

Idiopathic portal hypertension (IPH) represents noncirrhotic portal hypertension of unknown etiology, mainly due to stenosis of peripheral portal veins. This study was performed to clarify the mechanism of portal venous stenosis in IPH from the viewpoint of the contribution of the endothelial to mesenchymal transition of the portal vein endothelium via transforming growth factor-β1 (TGF-β1)/Smad activation. *In vitro* experiments using human dermal microvascular endothelial cells demonstrated that TGF-β1 induced myofibroblastic features in human dermal microvascular endothelial cells, including spindle cell morphology, reduction of CD34 expression, and induction of S100A4, α-smooth muscle actin, and COL1A1 expression, as well as the increased nuclear expression of phospho-Smad2. Bone morphogenic protein-7 preserved the endothelial phenotype of human dermal microvascular endothelial cells. Immunohistochemical analysis showed that endothelial cells of the peripheral portal veins in IPH were characterized by the decreased expression of CD34 and the enhanced nuclear expression of phospho-Smad2; these results also confirmed the expression of S100A4 and COL1A1 in the portal vein endothelium. Serum TGF-β1 levels in patients with IPH were significantly higher than those of healthy volunteers and patients with chronic viral hepatitis/liver cirrhosis, while an elevation of serum bone morphogenic protein-7 levels was not observed. These results suggest that the endothelial to mesenchymal transition of the portal venous endothelium via TGF-β1/Smad activation is associated with portal venous stenosis in IPH, and bone morphogenic protein-7 may therefore be a suitable therapeutic candidate for IPH. ***(Am J Pathol 2009, 175:616–626; DOI: 10.2353/ajpath.2009.081061)***

Idiopathic portal hypertension (IPH) is a condition of noncirrhotic presinusoidal portal hypertension of unknown etiology, primarily affecting adults.[1–3] Clinical presentations of IPH include splenomegaly, pancytopenia, gastroesophageal varices, and subcapsular parenchymal atrophy of the liver.[1] Histologically, phlebosclerosis and stenosis of peripheral portal veins associated with dense portal fibrosis are common and characteristic findings of IPH, accounting for portal hypertension due to presinusoidal block.[4–6] Hepatic function tends to be well preserved even at an advanced disease stage, but hepatic failure can lead to fatal outcome in some patients.[7] To date, a radical treatment is not available other than liver transplantation,[8,9] because the mechanism of portal venous stenosis of IPH has not been clarified.

IPH in patients is reported to be complicated with collagen vascular diseases such as systemic sclerosis.[10,11] Systemic sclerosis is a disease that causes excessive collagen production and deposition, vascular damage, and inflammation in multiple organs including skin, lung, and the gastrointestinal tracts.[12] Patients with

Supported by the Japanese Study Group of Intrahepatic Hemodynamics Alterations (Chairmen: Professor Makoto Hashizume, Kyushu University Graduate School of Medicine, Fukuoka; Professor Fuminori Moriyasu, Tokyo Medical School, Tokyo, Japan).

A.K. and Y.S. contributed equally to this work.

Accepted for publication May 5, 2009.

Address reprint requests to Yasuni Nakanuma, MD, PhD, Department of Human Pathology, Kanazawa University Graduate School of Medicine, 13-1 Takara-machi, Kanazawa 920-8640, Japan. E-mail: pbcpsc@kenroku.kanazawa-u.ac.jp.

the disease show an increased deposition of collagen types I and III in various organs, with type I being the most abundant.[12] Transforming growth factor-β (TGF-β) contributes greatly to the fibrotic processes, and elevation of circulating TGF-β level has been reported in patients with systemic sclerosis.[13,14] Although excessive collagen deposition in systemic sclerosis appears to be mediated by complex networks of various factors, one possible mechanism of the cutaneous fibrogenesis is that dermal microvascular endothelial cells transform into myofibroblastic cells, thereby contributing to the collagen deposition in the dermis.[15,16]

Recently, it has been described with increasing frequency that vascular endothelial cells have an ability to acquire matrix-producing myofibroblastic features, providing proof of principle for the process of endothelial to mesenchymal transition (EndMT).[17–19] EndMT is a phenomenon reported to occur during embryonic cardiovascular development,[20,21] and also occur under several pathological conditions including cardiac fibrosis and carcinoma-associated interstitial fibrosis.[17,18] EndMT is a phenotypic conversion characterized by the down-regulation of vascular endothelial markers such as CD31 and von Willebrand factor, and the emergence of myofibroblastic markers such as S100A4/fibroblast-specific protein-1 and α-smooth muscle actin (α-SMA).[16–18] TGF-β1 acts as a potent inducer of EndMT both *in vitro* and *in vivo*.[17,18,20]

TGF-β binds to TGF-β receptor type II (TβR-II), and it recruits the TGF-β receptor type I (TβR-I). TβR-I subsequently phosphorylates Smad2 and Smad3, which form hetero-oligomers with Smad4. They translocate from the cytoplasm to the nucleus, where they regulate transcription of target genes.[22] Bone morphogenic protein-7 (BMP7) is a member of the TGF-β superfamily, and a promising TGF-β antagonist.[23,24] BMP7 binds and activates BMP type II receptor that subsequently form complex with BMP receptor type IA. The receptors activated by BMP7 phosphorylate Smad1, 5 and 8, which counteract Smad2/3 phosphorylation by TGF-β. Indeed, BMP7 has been shown to inhibit EndMT in a mouse model of cardiac fibrosis.[17]

In most types of chronic liver disease, hepatic fibrosis is mediated by myofibroblasts, which generally originate from hepatic stellate cells. Portal fibroblasts and bone-marrow derived fibrocytes are other candidates of cell types of myofibroblast precursor in the liver.[25] Given the facts that systemic sclerosis is a clinical complication of IPH, and EndMT is one of the possible causative mechanism of excessive collagen deposition in systemic sclerosis, it is plausible that, in IPH, stenosis of peripheral portal veins with dense collagenous fibrosis around them is mediated by EndMT of the endothelial cells of portal vein, and the endothelial cell may be another contributor of the portal fibrosis.

To clarify this, the involvement of EndMT in portal venous stenosis of IPH was examined by the use of microvascular endothelial cells *in vitro*, and by means of histological analysis using liver tissue sections of IPH. Measurement of the serum TGF-β1 and BMP7 levels was also performed using samples obtained from IPH patients.

Materials and Methods

This human study was performed with the approval of the ethics committee of Kanazawa University Graduate School of Medicine.

Cell Culture

Human dermal microvascular endothelial cells (HMVEC) were purchased from Cell Applications, Inc. (San Diego, CA), and were maintained with endothelial growth medium (CADMEC growth medium, Cell Applications, Inc.). HMVECs were then treated with either TGF-β1 (10 ng/ml; R&D systems, Inc., Minneapolis, MN) alone or in combination with BMP7 (up to 100 ng/ml; R&D systems, Inc.) for 5 days, and phenotypic changes of HMVECs were examined as described below. Experiments were conducted with HMVECs at passages 2 to 4.

Reverse Transcription-PCR and Quantitative Real-time PCR

Reverse transcriptase (RT) PCR was performed using total RNA (1 μg) extracted from HMVECs. Total RNA was extracted using an RNA extraction kit (RNeasy mini; Qiagen, Tokyo, Japan) and was used to synthesize cDNA with reverse transcriptase (ReverTra Ace; Toyobo Co., Osaka, Japan). The sequences of the primers and conditions for PCR used are shown in Table 1. The PCR products were subjected to 2% agarose gel electrophoresis and stained with ethidium bromide.

Quantitative real-time PCR was performed according to a standard protocol using the SYBR Green PCR Master Mix (Toyobo Co.) and ABI Prism 7700 Sequence Detection System (PE Applied Biosystems, Warrington, UK). Cycling conditions were incubation at 50°C for 2 minutes, 95°C for 10minutes, and 40 cycles of 95°C for 15 seconds and 60°C for 1 minute. Fold difference compared with glyceraldehyde-3-phosphate dehydrogenase expression was calculated.

Western Blot Analysis

Total proteins were extracted from HMVEC using T-PER protein extraction reagent (Pierce Chemical Co., Rockford, IL). First, 5 μg of the protein was subjected to 10% SDS-polyacrylamide gel electrophoresis, and then electrophoretically transferred on to a nitrocellulose membrane. The membrane was incubated with primary antibodies against CD31 (1:200, JC70A, mouse monoclonal; DakoCytomation, Glostrup, Denmark), CD34 (1:250, QBEND10, mouse monoclonal; Immunotech, Marseilles, France), S100A4 (1:200, rabbit polyclonal; Abcam Inc., Cambridge, MA), α-SMA (1:200, 1A4, mouse monoclonal; DakoCytomation), pro-COL1A1 (1:200, goat polyclonal, Santa Cruz Biotechnology, Inc., Santa Cruz, CA), and actin (1:3000, AC-15, mouse monoclonal; Abcam

Table 1. Sequences of the Primers and PCR Conditions Used in this Study

Gene	Sequences	Annealing temperature (°C)	PCR cycles	Product size (bp)
TβR-I	5′-GGCCATTTACACTGAATGAG-3′ 5′-GGCTTAGAAATGGCCCAAAA-3′	55	40	386
TβR-II	5′-GTGGAGACACTTACAAAGCT-3′ 5′-GAAACTTGGGCTAACTGAGA-3′	55	40	250
BMP-RIA	5′-GGTTTCATAGCGGCAGACAT-3′ 5′-CTTTCCTTGGGTGCCATAAA-3′	55	40	198
BMP-RII	5′-GCTAAAATTTGGCAGCAAGC-3′ 5′-CTTGGGCCCTATGTGTCACT-3′	55	40	224
CD31	5′-CCTGCTAAGTTAATGTTGGG-3′ 5′-GAAAAAACCAGCCTCTAACC-3′	62	40	269
CD34	5′-CCAATCTGACCTGAAAAAGC-3′ 5′-CCACCGTTTTCCGTGTAATA-3′	55	30	216
S100A4	5′-GGTGACAAGTTCAAGCTCAA-3′ 5′-CTGGGAAGCCTTCAAAGAAT-3′	55	40	214
α-SMA	5′-GAAATGAACGTTTCCGCTGC-3′ 5′-CAGACAGAGTATTTGCGCTC-3′	62	40	268
COL1A1	5′-GTCTTCTGCAACATGGAGAC-3′ 5′-CAGTGGTAGGTGATGTTCTG-3′	62	40	245
GAPDH	5′-GAGTCAACGGATTTGGTCGT-3′ 5′-TTGATTTTGGAGGGATCTC-3′	55	30	240

Inc.). The protein expression was detected using an EnVision+ system (DakoCytomation) and a HISTOFINE system (Nichirei, Tokyo, Japan). 3,3′-diaminobenzidine tetrahydrochloride was used as the chromogen. Semiquantitative analysis of the results was performed using NIH J image software (National institutes of Health, Bethesda, MD). The fold difference compared with actin expression was calculated.

Immunocytochemistry

HMVECs were fixed with 4% paraformaldehyde for 15 minutes, and permeabilized for 3 minutes with 0.1% Triton X-100. After blocking, the cells were incubated for 1 hour at room temperature with primary antibodies against CD34 (1:200, Immunotech), S100A4 (1:100, Abcam Inc.), α-SMA (DakoCytomation), pro-COL1A1 (1:100, goat polyclonal, Santa Cruz Biotechnology, Inc.), and phospho-Smad2 (pSmad2) (1:100, Ser465/467, rabbit polyclonal; Cell Signaling Technology, Inc., Danvers, MA). The protein expression was detected using the alkaline phosphatase-labeled polymer, the HISTOFINE system (Nichirei). Color development was performed using the Vector Red alkaline phosphatase substrate kit (Vector Laboratories, Burlingame, CA), and nuclei were stained with 4′6-diamidino-2-phenylindole. The signals were detected under immunofluorescence confocal microscopy.

Liver Specimens

A total of 44 liver specimens were used. Twenty-four specimens corresponded to IPH. Clinicopathological features of IPH cases were summarized in Table 2. Both liver biopsy and autopsy materials were included. The IPH livers of autopsy cases were collected as previously described, and all autopsy livers were obtained at an advanced disease stage corresponding to Stage III or Stage IV.[1,7] Histology of the liver confirmed the diagnosis of IPH, and five cases corresponded to incomplete septal cirrhosis. Complication of systemic sclerosis was observed in three cases.

As controls, liver specimens obtained from patients with chronic viral hepatitis/liver cirrhosis (CVH/LC) (n = 10), and histologically normal livers (NL) (n = 10) were used. The causes of CVH/LC were viral infection of hepatitis B (n = 2) and hepatitis C (n = 8). NL specimens were obtained from patients undergoing a partial hepatectomy for the diseases other than hepatobiliary disorders such as metastatic colon cancer, and macroscopically and microscopically normal areas were used.

Immunohistochemistry

Liver specimens were fixed with neutral formalin, and 4-μm thick paraffin-embedded tissue sections were pre-

Table 2. Clinicopathological Features of IPH Cases Used for Histological Analysis

N	Age (years)	Sex (male:female)	Specimen (biopsy:autopsy)	Splenomegaly	Esophageal varices	Liver weight* (g)	Splenic weight* (g)	Liver fibrosis†	Systemic sclerosis
24	59 ± 20	7:17	6:18	22(92%)	17(77%)	779 ± 293	378 ± 176	5(21%)	3(13%)

*Liver and splenic weight were the value of autopsy cases.
†Liver fibrosis corresponded to incomplete septal cirrhosis.

pared. Immunostaining was performed using primary antibodies against TβR-I (sc-398, rabbit polyclonal; Santa Cruz Biotechnology, Inc., Santa Cruz, CA), TβR-II (sc-220, rabbit polyclonal; Santa Cruz Biotechnology, Inc.), CD34 (Immunotech), and pSmad2 (Cell Signaling Technology, Inc.). After deparaffinization, antigen retrieval was performed by incubating with 1 mg/ml of trypsin for 10 minutes at 37°C for TβR-I and TβR-II staining, and by incubating with 20 mg/ml of proteinase K for 6 minutes at room temperature for pSmad2 staining. To block the activity of endogenous peroxidase, sections were immersed in 0.3% hydrogen peroxidase in methanol for 20 minutes at room temperature. After pretreatment with blocking serum (DakoCytomation), sections were incubated overnight at 4°C with individual primary antibodies; TβR-I (1:50), TβR-II (1:50), CD34 (1:200), and pSmad2 (1:100). Then sections were incubated with secondary antibodies conjugated to peroxidase-labeled polymer, using the EnVision+ system (DakoCytomation). Color development was performed using 3,3′-diaminobenzidine tetrahydrochloride and the sections were slightly counterstained with hematoxylin. Negative controls were done by substitution of the primary antibodies with nonimmunized serum, resulted in no signal detection.

Double Immunofluorescence Staining

Double immunofluorescence staining of CD34 and S100A4, CD34 and α-SMA, and CD34 and COL1A1 was performed for the liver sections. Deparaffinized sections were incubated 1 hour at room temperature with the anti-CD34 antibody (1:200, Immunotech). The sections were incubated with secondary antibodies conjugated to alkaline phosphatase-labeled polymer, the HISTOFINE system (Nichirei). Color development was performed using the Vector Red alkaline phosphatase substrate kit (Vector Laboratories, Burlingame, CA). Then, antigen retrieval was performed by incubating with 20 mg/ml of proteinase K for 6 minutes at room temperature for the staining of S100A4. After microwaving in 10 mmol/L citrate buffer pH 6.0 for 10 minutes, the sections were incubated overnight at 4°C with the anti-S100A4 antibody (1:100, Abcam Inc.), the anti-α-SMA antibody (1:200, DakoCytomation), and the anti-pro COL1A1 antibody (1:100, Santa Cruz Biotechnology, Inc.). Alexa Fluor 488 (10 μg/ml; Molecular Probes, Eugene, OR) was used as a secondary antibody. Nuclei were stained with 4′6-diamidino-2-phenylindole, and the sections were observed under immunofluorescence confocal microscopy.

Histological Assessment

Semiquantitative analysis was performed for the sections stained with the anti-CD34 antibody. In each section, a total of 20 peripheral portal tracts were randomly selected. For liver biopsy specimens, all portal tracts in the specimen were evaluated, because they usually did not contain 20 portal tracts. As described later, the endothelial cells of peripheral portal vein of IPH frequently showed reduced immuno-expression of CD34. The CD34 signal intensity of the endothelial cells was compared between the portal vein and the escorting hepatic artery in the same portal tract. The CD34 signal intensity was regarded as being reduced when less CD34 expression was observed in more than 2/3 circumference of one portal vein. The percentage of the number of portal veins with reduced CD34 expression was calculated in each case, and was defined as CD34-reduction index. The histological assessment was performed by two independent investigators (A.K. and Y.S.).

For immunostained sections of pSmad2, a total of 100 nuclei of the endothelial cells of peripheral portal vein were randomly selected in each section. The percentage of the endothelial cells positive for pSmad2 was determined, and was defined as pSmad2-labeling index. For the determination of pSmad2 expression in HMVECs, a total of 100 nuclei of HMVECs immunostained with the anti-pSmad2 antibody were evaluated, and pSmad2-labeling index was calculated in the same manner.

Enzyme-Linked Immunosorbent Assay

The serum TGF-β1 and BMP7 levels of 66 samples obtained from 57 IPH patients were determined using enzyme-linked immunosorbent assay kits (Quantikine Human TGF-β1 Immunoassay and Quantikine Human BMP7 Immunoassay; R&D Systems, Inc.) according to the manufacturer's instructions. As controls, serum samples obtained from 16 healthy volunteers and 19 patients with CVH/LC (hepatitis B, $n = 9$; hepatitis C, $n = 10$) were used. Samples were added to a 96-well plate coated with a monoclonal antibody for TGF-β1 or BMP7, and incubated for 2 hours at room temperature. After washing, the plate was incubated with anti-TGF-β1 or anti-BMP7 antibody conjugated to horseradish peroxidase for 2 hours at room temperature. Color development was performed using a substrate solution for 30 minutes and the absorbance at 450 nm was measured.

Statistics

The data were expressed as the mean ± SD. Statistical significance was determined using the Mann-Whitney *U*-test and the Pearson correlation test. A P value less than 0.05 was accepted as the level of statistical significance.

Results

Effects of TGF-β1 and BMP7 on Cellular Phenotype of HMVECs

RT-PCR analysis showed that HMVECs expressed receptors for TGF-β (TβR-I, TβR-II) and BMP7 (BMP receptor type IA, BMP type II receptor) (Figure 1A). In this study, CD31 and CD34 were used as markers of vascular endothelial cells, and S100A4 and α-SMA as markers of myofibroblastic cells. Treatment of HMVECs with TGF-β1 significantly reduced the expression of CD34 mRNA in HMVECs, and induced mRNA expression of S100A4,

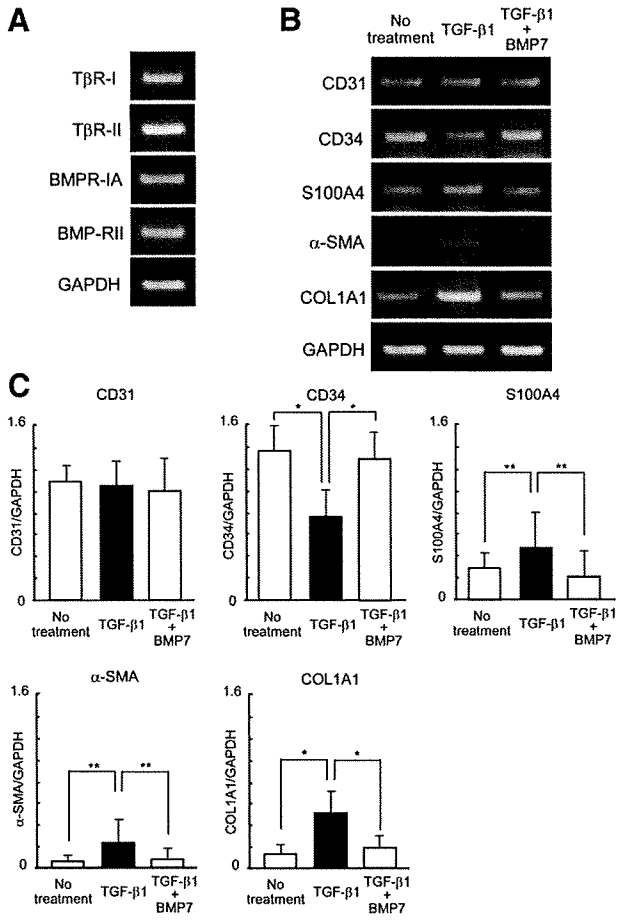

Figure 1. Effects of TGF-β1 and BMP7 on cellular phenotype of HMVECs at the mRNA level. HMVECs were treated with TGF-β1 (10 ng/ml) alone or in combination with BMP7 (100 ng/ml) for 5 days, and phenotypic changes were examined using RT-PCR as described in the *Materials and Methods*. HMVECs expressed receptors for TGF-β (TβR-I, TβR-II) and BMP7 (BMP receptor type IA, BMP type II receptor) (**A**). RT-PCR (**B**) and real-time PCR (**C**) showed that treatment of HMVECs with TGF-β1 reduced the expression of CD34 mRNA, and induced the mRNA expression of S100A4, α-SMA, and COL1A1. All of these changes of HMVECs following TGF-β1 treatment were inhibited by the addition of BMP7 in the culture medium (**B, C**). The data represent three independent experiments (**A, B**), and the mean ± SD of six per group (**C**). $^{*}P < 0.01$; $^{**}P < 0.05$.

α-SMA, and COL1A1, while mRNA expression of CD31 was unchanged (Figure 1, B and C). Western blot analysis showed that proteins of the molecules showed similar changes to those of mRNA following TGF-β1 treatment, and semiquantitative analysis of the Western blotting confirmed this tendency (Figure 2, A and B). All of these phenotypic changes of HMVECs following TGF-β1 treatment were blocked by the addition of BMP7 in the culture medium (Figures 1, B and C, and 2, A and B). In addition, BMP7 reduced TGF-β1-induced COL1A1 expression in HMVEC in a dose-dependent fashion (Figure 2C).

Morphological and Phenotypic Alterations of HMVEC by TGF-β1 and BMP7

In the endothelial growth medium, HMVEC grew in a form of epithelioid, sheet-like appearance under the phase-contrast microscopy. Following 5-day treatment with TGF-β1, the cellular morphology of HMVEC changed from epithelioid into spindle-shaped appearance (Figure 3). Immunocytochemistry showed that the spindle-shaped HMVEC following TGF-β1 treatment exhibited reduced expression of CD34, and increased expression of S100A4, α-SMA, and COL1A1 (Figure 3), which were consistent with the results of RT-PCR and Western blot analysis. TGF-β1 treatment increased the expression of pSmad2 in the nuclei of HMVECs (Figure 3), and the percentage of HMVECs positive for pSmad2 were significantly increased from 8.2 ± 6.3% to 52.7 ± 18.3% following the treatment. Again, the addition of BMP7 in the culture medium inhibited the morphological and phenotypic conversion of HMVECs by TGF-β1 (Figure 3). These results indicated that TGF-β1 could induce myofibroblastic features in HMVECs, and BMP7 antagonized the effects of TGF-β1.

Reduction of CD34 Expression in Portal Vein Endothelium of IPH Livers

Immunostaining of liver sections demonstrated that both TβR-I and TβR-II were diffusely expressed in the liver including portal vein endothelium of IPH (Figure 4A), as well as NL and CVH/LC. Immunohistochemical expression of CD34 was observed in the endothelial cells of portal vein, hepatic artery, and hepatic vein in all liver specimens without exceptions. The signal intensity of CD34 immunostaining was almost equal among these vessels in NL (Figure 4B). In IPH, reduction of CD34 expression in the endothelial cells of peripheral portal vein was frequently observed when compared with those of the escorting hepatic artery in the same portal tract (Figure 4B). The reduction of CD34 expression was observed in peripheral portal veins of IPH regardless of the presence or absence of luminal narrowing. In CVH/LC, CD34 expression in the portal endothelial cells tended to be preserved in most of the cases (Figure 4B), but several cases showed reduction of CD34 expression. Semiquantitative analysis of the results of CD34 immunostaining was performed as described in the *Materials and Methods*. As shown in Figure 4C, the CD34-reduction index was significantly increased in IPH, when compared with that of NL and CVH/LC.

Enhanced Expression of pSmad2 in IPH Livers

Positive immunostaining for pSmad2 were rarely seen in sections of NL (Figure 4B). By contrast, many IPH cases showed diffuse and strong nuclear expression of pSmad2 throughout the liver, including portal vein endothelium, hepatocytes, and biliary epithelial cells (Figure 4B). Several cases of CVH/LC showed positive immunohistochemical signals of pSmad2 in the liver, but most of the cases lacked its expression (Figure 4B).

Semiquantitative analysis of the immunohistochemical results showed that the expression of pSmad2 was negligible in NL, whereas IPH livers showed a high incidence of pSmad2 expression in portal vein endothelium (73.8 ± 25.6%) (Figure 4D). In CVH/LC, the pSmad2-labeling

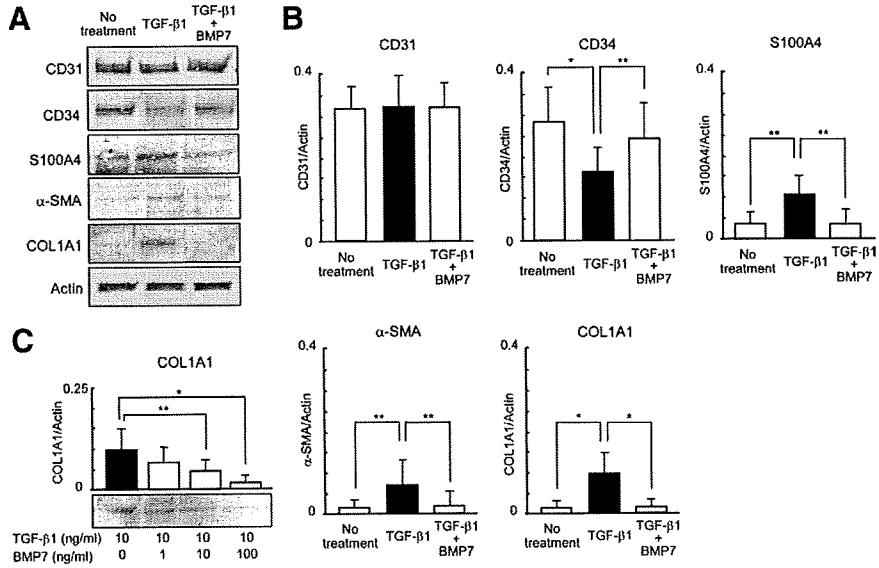

Figure 2. Effects of TGF-β1 and BMP7 on cellular phenotype of HMVECs at the protein level. HMVECs were treated with TGF-β1 (10 ng/ml) alone or in combination with BMP7 (100 ng/ml) for 5 days, and phenotypic changes were examined by Western blotting using protein extracts from HMVEC. Consistent with the RT-PCR results, TGF-β1 reduced the expression of CD34 protein, and induced the protein expression of S100A4, α-SMA and COL1A1, and the addition of BMP7 inhibited these phenotypic changes (**A**). Semiquantitative analysis of the Western blotting confirmed this tendency (**B**). BMP7 inhibited TGF-β1-induced COL1A1 protein expression in a dose-dependent manner (**C**). The data represent five independent experiments (**A**), and the mean ± SD of five per group (**B, C**). $^{*}P < 0.01$; $^{**}P < 0.05$.

index was 12.4 ± 4.0%, and there was a statistically significant difference between the index of IPH and CVH/LC groups. This study examined three cases of systemic sclerosis complicated with IPH. Interestingly, these cases of systemic sclerosis exhibited high value of the pSmad2-labeling index as well as the CD34-reduction index (Figure 4, C and D, data indicated by white circles). When the pSmad2-labeling index was plotted against the CD34-reduction index for all 44 cases, they showed a fine liner correlation (Figure 4E), suggesting a causal relationship between the enhanced expression of pSmad2 and the reduced expression of CD34 in portal vein endothelium.

In this study, liver specimens of IPH included both liver biopsy and autopsy materials. Because all autopsy livers of IPH were obtained at an advanced disease stage, the specimens of liver biopsy might reflect pathological changes at an earlier disease stage of IPH, when compared with those of autopsy livers. In autopsy IPH livers, the CD34-reduction index and the pSmad2-labeling index were 68.3 ± 19.9% and 67.9 ± 26.9%, respectively, while those of biopsy livers were 69.2 ± 9.7% and 91.8 ± 6.7%, respectively. These results indicated that the occurrence of reduction of CD34 expression and induction of pSmad2 expression in the portal vein endothelium was not a phenomenon limited to the end stage of the disease, and might be closely associated with the disease progression.

Colocalization of CD34 and Mesenchymal Markers in Portal Vein Endothelium of IPH Livers

Co-expression of CD34 and S100A4 was observed in portal vein endothelium of IPH (Figure 5, arrow), but the

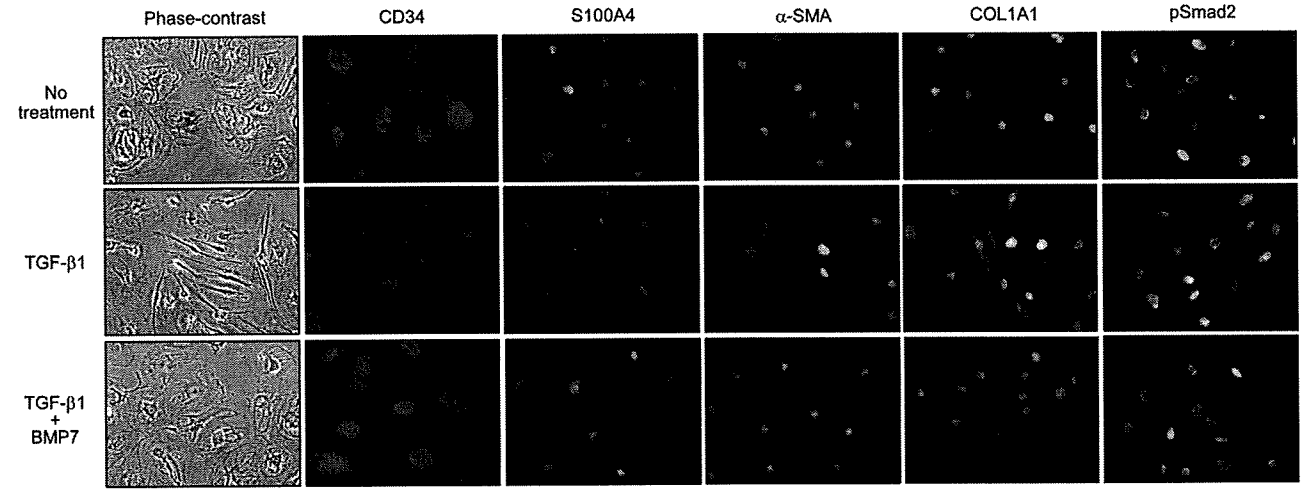

Figure 3. Morphological and phenotypic alterations of HMVECs by TGF-β1 and BMP7. HMVECs grew in a form of epithelioid, sheet-like appearance under the phase-contrast microscopy, and a 5-day treatment with TGF-β1 (10 ng/ml) changed the cellular morphology of HMVECs from epithelioid into spindle-shaped appearance. Immunostaining showed that the spindle-shaped HMVECs following TGF-β1 treatment showed reduced expression of CD34, and increased expression of S100A4, α-SMA, COL1A1, and pSmad2. Addition of BMP7 (100 ng/ml) in the culture medium inhibited the phenotypic changes of HMVECs by TGF-β1. The protein expression was visualized by a Vector Red reaction under immunofluorescence confocal microscopy, and nuclei were stained with 4′6-diamidino-2-phenylindole (blue). Original magnification ×1000.

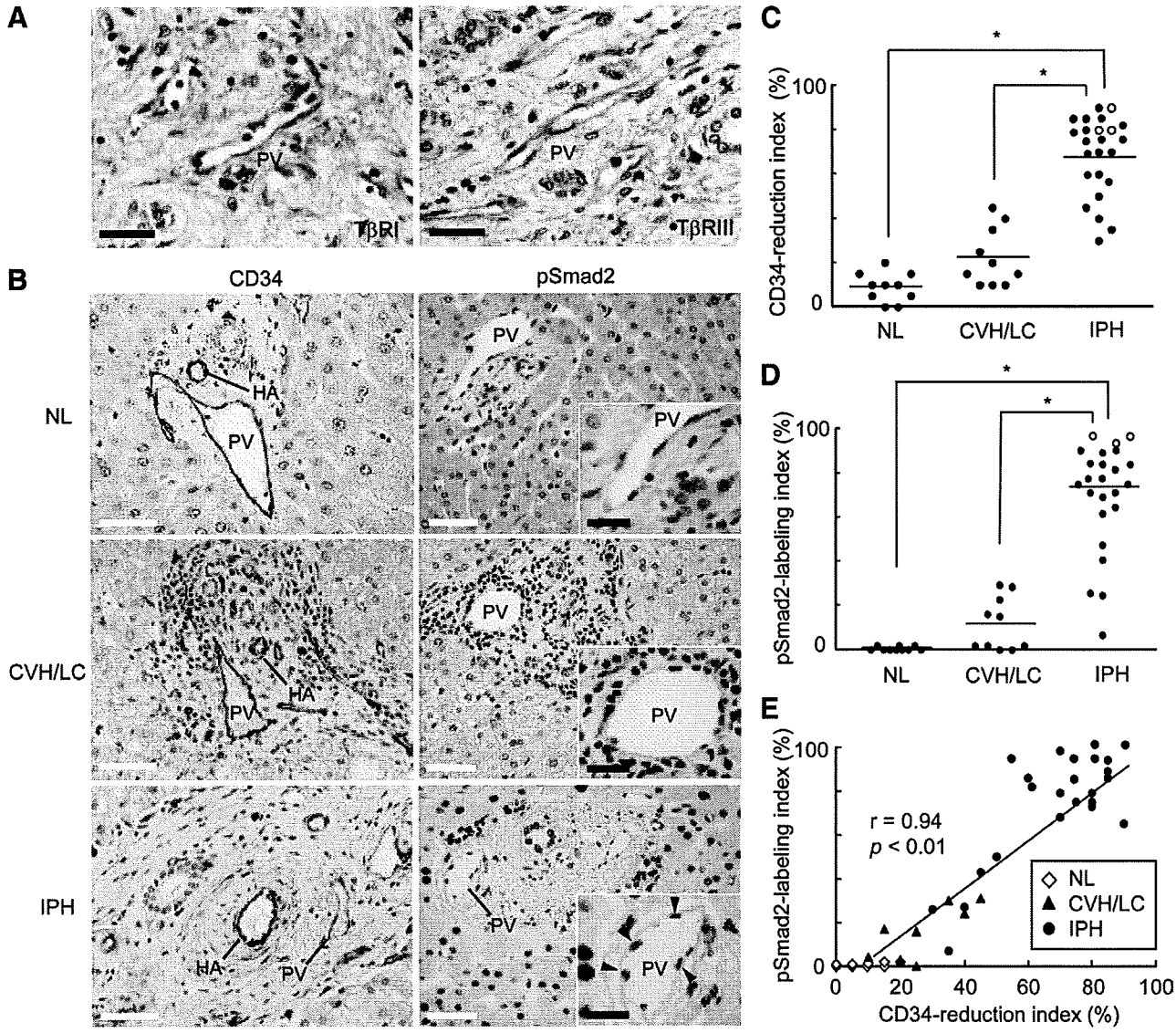

Figure 4. Reduction of CD34 expression and induction of pSmad2 expression in portal vein endothelium of IPH livers. Immunostaining of TGF-β receptors (TβR-I, TβR-II), CD34 and pSmad2 was performed for liver sections of normal liver (NL), chronic viral hepatitis/liver cirrhosis (CVH/LC) and idiopathic portal hypertension (IPH). TβR-I and TβR-II were diffusely expressed in the portal vein endothelium of IPH (**A**), as well as NL and CVH/LC. Endothelial cells of peripheral portal vein of IPH showed reduced expression of CD34, and increased expression of pSmad2 (**B**). The CD34-reduction index and the pSmad2-labeling index of portal vein endothelium were determined as described in the *Materials and Methods* section. Portal vein endothelium of IPH showed a significant reduction of CD34 expression (**C**) and a significant induction of pSmad2 (**D**) when compared with those of NL and CVH/LC. The data of white circles represent those from the cases of IPH complicated with systemic sclerosis (**C, D**). The CD34-reduction index and the pSmad2-labeling index showed a fine liner correlation (**E**). **Arrowheads** indicate nuclei of pSmad2-positive portal vein endothelium (**B**). HA, hepatic artery. PV, portal vein. White bars = 50 μm; black bars = 20 μm. $^*P < 0.01$.

expression was limited in a small number of portal veins. Portal vein endothelium of NL and CVH/LC lacked double-positive signals of CD34 and S100A4 (Figure 5). Co-expression of CD34 and α-SMA was rarely seen in all experimental groups (data not shown). Double immunofluorescence staining of CD34 and COL1A1 showed that portal vein endothelium of IPH occasionally co-expressed CD34 and COL1A1 (Figure 5, arrowheads), and the portal veins showing double-positive signals irregularly distributed in an individual liver independently of the presence or absence of luminal narrowing. Portal vein endothelium of NL and CVH/LC typically lacked such double-positive signals (Figure 5).

Elevation of Circulating TGF-β1 Level in IPH

The serum TGF-β1 and BMP7 levels of 66 samples obtained from 57 IPH patients, 16 healthy volunteers, and 19 patients with CVH/LC were determined using an enzyme-linked immunosorbent assay. The serum TGF-β1 level of healthy controls, CVH/LC, and IPH were 40.3 ± 17.6 ng/ml, 29.3 ± 10.8 ng/ml, and 53.0 ± 23.4 ng/ml, respectively, and the TGF-β1 level in IPH patients was significantly higher than the value of the other two groups (Figure 6A). While the serum BMP7 level of healthy controls, CVH/LC, and IPH were 5.0 ± 2.4 pg/ml, 22.5 ± 12.4 pg/ml, and 6.6 ± 5.5 pg/ml, respectively, and the serum

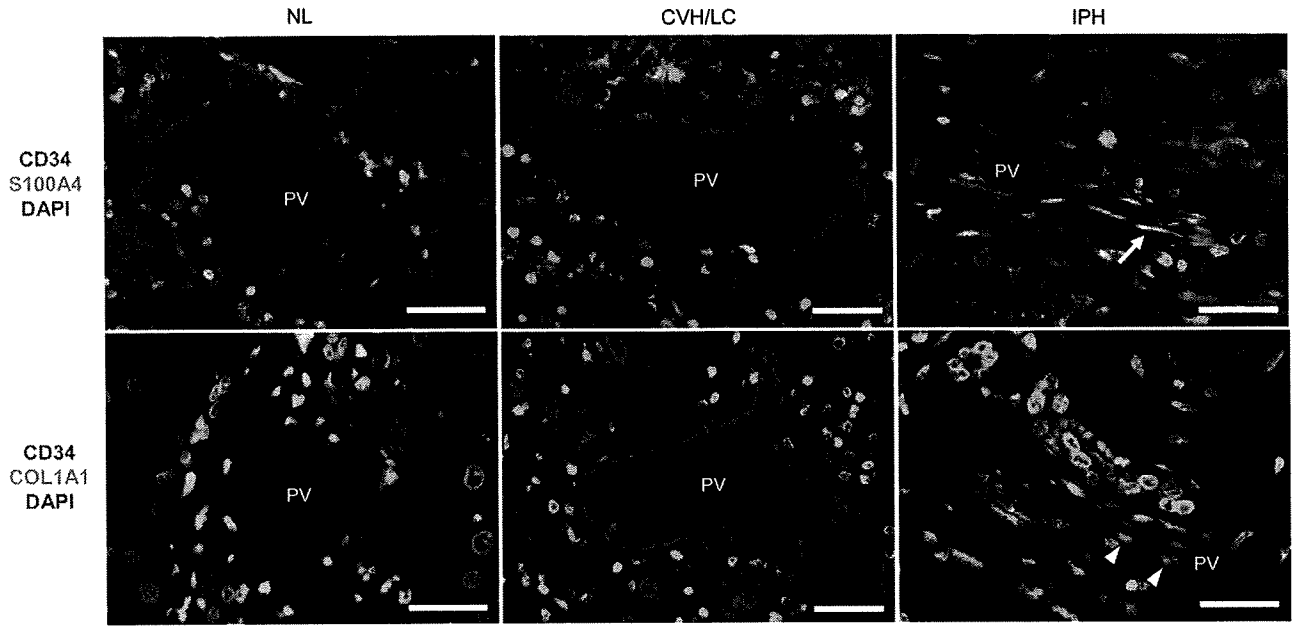

Figure 5. Colocalization of CD34 and mesenchymal markers in portal vein endothelium of IPH livers. Double immunofluorescence staining of CD34 and S100A4 protein, and CD34 and COL1A1 was performed for liver sections of normal liver (NL), chronic viral hepatitis/liver cirrhosis (CVH/LC), and idiopathic portal hypertension (IPH). Figures shown were merged images in which the expression of CD34 was colored in red, and the expression of S100A4 and COL1A1 was colored in green. Nuclei were stained with 4′6-diamidino-2-phenylindole. Coexpression of CD34 and S100A4 was observed in portal vein endothelium of IPH (**arrow**), but the expression was limited in a small number of portal veins of IPH. Portal vein endothelium of NL and CVH/LC typically lacked double-positive signals of CD34 and S100A4. Portal vein endothelium of IPH occasionally showed colocalization of CD34 and COL1A1 (**arrowheads**). PV, portal vein. White bars = 30 μm.

BMP7 level in patients with CVH/LC showed a significant increase compared with those of the other two groups (Figure 6B). When the serum TGF-β1 level was plotted against the serum BMP7 level for all cases examined, a significant inverse correlation was observed between them (Figure 6C).

Discussion

In this study, TGF-β1 induced phenotypic conversion of HMVECs into collagen-producing myofibroblast-like cells, and BMP7 preserved the endothelial phenotype. *In vivo*, endothelial cells of peripheral portal vein of IPH were characterized by the decreased expression of CD34, and the enhanced expression of pSmad2 and COL1A1. Importantly, the serum TGF-β1 level of IPH patients was significantly elevated when compared with the value of the healthy controls and CVH/LC. These results suggest that EndMT of the portal vein endothelium via TGF-β1/Smad activation is closely associated with the pathogenesis of portal venous stenosis of IPH. Our hypothesis on the mechanism of portal venous stenosis of IPH is illustrated in Figure 7.

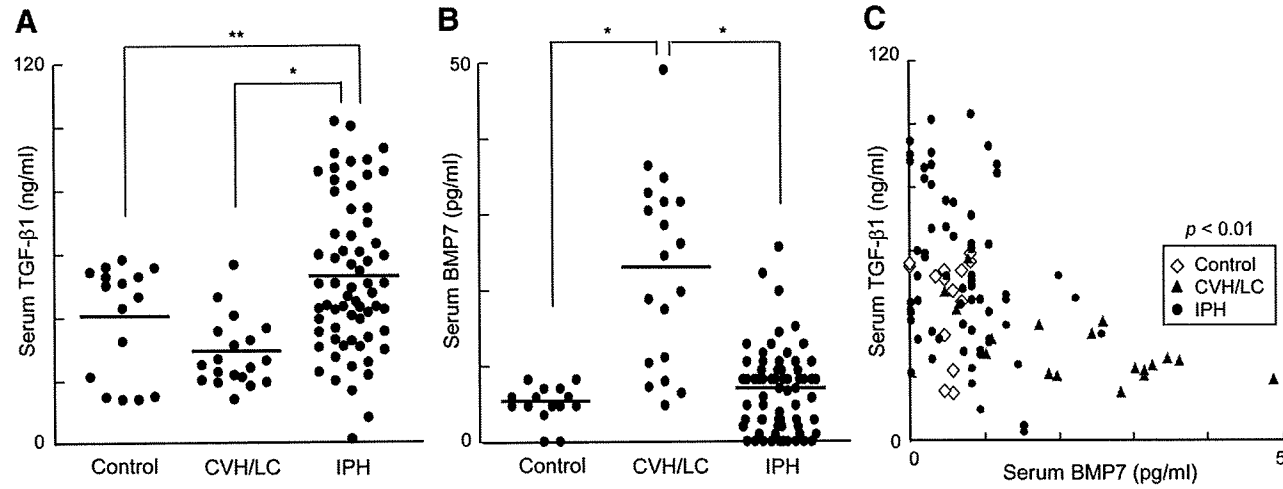

Figure 6. Elevation of circulating TGF-β1 levels in IPH. The serum TGF-β1 and BMP7 levels of 66 samples obtained from 57 patients with idiopathic portal hypertension (IPH), 16 healthy volunteers, and 19 patients with chronic viral hepatitis/liver cirrhosis (CVH/LC) were determined using an enzyme-linked immunosorbent assay. Serum obtained from IPH patients contained a significantly high level of TGF-β1 when compared with that of healthy controls and CVH/LC (**A**), while the serum BMP7 level in patients with CVH/LC showed a significant increase compared with those of the other two groups (**B**). When the serum TGF-β1 level was plotted against the serum BMP7 level for all cases examined, a significant inverse correlation was observed between them (**C**). $^{*}P < 0.01$; $^{**}P < 0.05$.

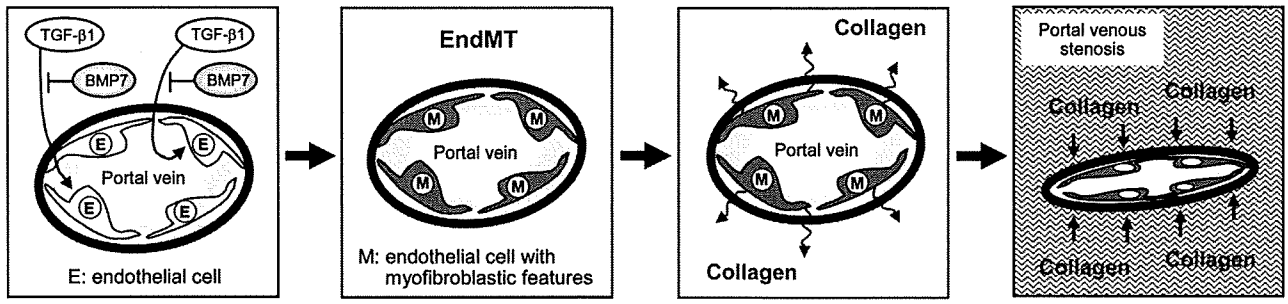

Figure 7. Proposed mechanism of the portal venous stenosis of IPH. TGF-β1 induces endothelial to mesenchymal transition (EndMT) of endothelial cells of peripheral portal vein of idiopathic portal hypertension (IPH). Endothelial cells acquire myofibroblastic features via Smad activation, and produce extracellular matrix molecules including collagen. Collagen depositions in peripheral portal tracts compress the portal veins, resulting in portal venous stenosis and presinusoidal portal hypertension. BMP7 may act as an inhibitor of EndMT by antagonizing the effects of TGF-β1.

Dense portal fibrosis with luminal narrowing of peripheral portal veins is a common histological hallmark of IPH.[1] Parenchymal fibrosis, such as pericellular fibrosis and slender fibrous septa from the portal tracts, leading to incomplete septal cirrhosis, is also observed in several cases of IPH.[1] Because α-SMA-positive activated hepatic stellate cells are focally fund in perisinusoidal area of IPH livers, parenchymal fibrosis may be explainable by the contribution of myofibroblasts.[1,5] However, α-SMA-positive myofibroblast-like cells are rarely seen in the peripheral portal tracts of IPH,[5,26] suggesting that other matrix-producing cells may exist in the portal tracts.

Since EndMT has been implicated in dermal fibrosis in patients with systemic sclerosis, a possible clinical manifestation of IPH,[10,15,16] we focused on EndMT of the portal vein endothelium as a mechanism of portal venous stenosis of IPH. *In vitro*, it has been reported that vascular endothelial cells acquire myofibroblastic features, such as an increase in S100A4/ fibroblast-specific protein-1, α-SMA and type I collagen expression in response to TGF-β1, which is accompanied by the reduced expression of vascular endothelial markers, CD31 and von Willebrand factor.[17,18] In fact, this study confirmed that TGF-β1 reduced the expression of CD34, and induced S100A4, α-SMA, and COL1A1 expression in HMVEC, which were accompanied by the increased nuclear labeling of pSmad2. In addition, portal vein endothelium of IPH showed the reduced CD34 expression and the increased nuclear expression of pSmad2. Although a question remains whether HMVEC and portal vein endothelium share the same endothelial phenotype, our data indicate that EndMT via TGF-β1/Smad activation is a possible mechanism of portal venous stenosis of IPH.

TGF-β1 is known to activate hepatic stellate cells, which in turn acquire myofibroblastic features and produce extracellular matrix proteins. This transition is a central process in LC due to various causes. However, no cirrhosis occurs in IPH despite the facts that activation of hepatic stellate cells occurs in focal areas of IPH livers, and incomplete septal cirrhosis is regarded as a late manifestation of IPH.[1,5] In systemic sclerosis, dermal fibroblasts shows hyperresponsiveness to TGF-β1, and the deficient expression of Smad7, an inhibitory Smad, may be responsible for the TGF-β hyperresponsiveness.[27] In addition, Smad6, another inhibitory Smad, is not expressed equally among cell types consisting the liver.[28] From these results, it is suggested that the responsiveness to TGF-β1 is different between portal vein endothelium and hepatic stellate cells of IPH; ie, portal vein endothelium of IPH may be hyperresponsive to TGF-β1 when compared with that of hepatic stellate cells, which may be due to the abnormalities of the expression of inhibitory Smads, accounting for the fact that no cirrhosis occurs in IPH.

In this study, only a small fraction of portal endothelial cells of IPH exhibited transformed features in pathological examinations. Similarly, previous studies have shown the percentage of fibroblast-specific protein-1/CD31 double-positive cells remained in 3% of total cells in a mouse model of cardiac fibrosis, although nuclear staining of pSmad2/3 was present in 30% of endothelial cells.[17] These results indicate that several but not all of the endothelial cells with positive nuclear expression of pSmad2 or pSmad2/3 undergo phenotypic changes into myofibroblast-like cells, which may lead to the uneven distribution of stenotic portal tracts in the liver of IPH. However, a precise mechanism remains to be studied. In addition, the induction of nuclear pSmad2 expression and the reduction of CD34 expression were observed even in peripheral portal veins without luminal narrowing of IPH. We speculate that these portal veins will gradually show luminal narrowing along with the collagen deposition around the portal veins, and these changes may slowly and disproportionally progress in the IPH liver.

Colocalization of CD34 and α-SMA was rarely seen in the portal vein endothelium of IPH. These observations were consistent with the results of previous studies regarding EndMT, showing that the occurrence of colocalization of CD31 and α-SMA in the vascular endothelium was a rare event *in vivo*, when compared with the frequency of the occurrence of colocalization of CD31 and S100A4/ fibroblast-specific protein-1.[18] Therefore, vascular endothelial cells may be able to acquire the features of myofibroblasts *in vitro*, but they do not necessarily differentiate into myofibroblasts themselves *in vivo*.

The elevated serum TGF-β1 level in IPH raises a question as to the cellular sources of TGF-β1. In the liver, hepatic stellate cells, macrophages, hepatocytes, and bile duct epithelial cells are candidates of cell types that produce TGF-β1.[29–31] The spleen is an organ that closely associates with the disease pathogenesis of IPH, and macrophages have been shown to produce TGF-β1 in

the spleen.[32,33] In cases of systemic sclerosis, myofibroblasts, fibroblasts, vascular endothelial cells, macrophages, lymphocytes, and platelets are potential sources of TGF-β1.[34–37] To determine cellular sources of TGF-β1 in IPH, further study is necessary. Also, the cellular sources of BMP7 are of interest, especially in patients with CVH/LC.

In IPH livers, hepatocytes, as well as portal vein endothelium, showed diffuse and strong immuno-expression of pSmad2, which probably reflected the elevation of the serum TGF-β1 level. In addition to its contribution to hepatic fibrosis, TGF-β1 has an effect of growth inhibition or apoptosis induction on hepatocytes.[28,38] Therefore, hepatic parenchymal atrophy frequently seen in IPH patients at an advanced disease stage may associate with the growth inhibitory effects of TGF-β1 on hepatocytes, as well as the circulatory disturbance of the liver.

TGF-β induces connective tissue growth factor (CTGF) in various systems, and hepatic stellate cells are the major cellular sources of CTGF in the liver during liver fibrogenesis.[39] In patients with IPH, the serum CTGF level is significantly elevated than the value in healthy volunteers, and overexpression of CTGF seems to be one of the most important features of IPH.[40] The major cellular sources of CTGF in the liver of IPH has been shown to be periductal mononuclear cells, but hepatic stellate cells of IPH livers lack CTGF expression.[5,40] In addition to CTGF, our data indicate that TGF-β is another novel factor involved in the pathogenesis of IPH.

From the view point of therapeutic interventions, it is important to note that BMP7 had striking effects on the preservation of endothelial phenotype. The inverse correlation between serum TGF-β1 and BMP7 levels in this study suggests a possibility that TGF-β1 and BMP7 may have an antagonistic effect on their expression to each other. Although the inverse correlation between serum TGF-β1 and BMP7 has not been recognized in the previous literature and the mechanism remains unknown, there is a possibility that the administration of BMP7 in patients with IPH may improve the elevation of serum TGF-β1 level, and BMP7 can be a candidate of therapeutic agents for IPH.

In conclusion, the present study demonstrated an involvement of TGF-β1 in the pathogenesis of IPH. Although the mechanism of deposition of extracellular matrix proteins other than collagen such as elastin in the peripheral portal tracts is not fully understood,[41] one plausible mechanism of the portal venous stenosis of IPH is due to excessive collagen deposition via EndMT of portal vein endothelium in response to TGF-β1. Our data indicate that TGF-β is a potential target of therapy of IPH, and BMP7 can be a possible therapeutic agent.

References

1. Nakanuma Y, Tsuneyama K, Ohbu M, Katayanagi K: Pathology and pathogenesis of idiopathic portal hypertension with an emphasis of the liver: Pathol Res Pract 2001, 197:65–76
2. Dhiman RK, Chawla Y, Vasishta RK, Kakkar N, Dilawari JB, Trehan MS, Puri P, Mitra SK, Suri S: Non-cirrhotic portal fibrosis (idiopathic portal hypertension): experience with 151 patients and review of the literature. J Gastroenterol Hepatol 2002, 17:6–16
3. Okudaira M, Ohbu M, Okuda K: Idiopathic portal hypertension and its pathology: Semin Liver Dis 1996, 22:59–72
4. Tsuneyama K, Ohba K, Zen Y, Sato Y, Niwa H, Minato H, Nakanuma Y: A comparative histological and morphometric study of vascular changes in idiopathic portal hypertension and alcoholic fibrosis/cirrhosis. Histopathology 2003, 43:55–61
5. Tsuneyama K, Kouda W, Nakanuma Y: Portal and parenchymal alterations of the liver in idiopathic portal hypertension: a histological and immunohistochemical study. Pathol Res Pract 2002, 198: 597–603
6. Nakanuma Y, Hoso M, Sasaki M, Terada T, Katayanagi K, Nonomura A, Kurumaya H, Harada A, Obata H: Histopathology of the liver in non-cirrhotic portal hypertension of unknown aetiology. Histopathology 1996, 28:195–204
7. Sawada S, Sato Y, Aoyama H, Harada K, Nakanuma Y: Pathological study of idiopathic portal hypertension with an emphasis on cause of death based on records of Annuals of Pathological Autopsy Cases in Japan. J Gastroenterol Hepatol 2007, 22:204–209
8. Dumortier J, Bizollon T, Scoazec JY, Chevallier M, Bancel B, Berger F, Ducerf C, Claudel-Bonvoisin S, Paliard P, Boillot O, Trepo C: Orthotopic liver transplantation for idiopathic portal hypertension: indications and outcome. Scand J Gastroenterol 2001, 36:417–422
9. Krasinskas AM, Eghtesad B, Kamath PS, Demetris AJ, Abraham SC: Liver transplantation for severe intrahepatic noncirrhotic portal hypertension. Liver Transpl 2005, 11:627–634
10. Tsuneyama K, Harada K, Katayanagi K, Watanabe K, Kurumaya H, Minato H, Nakanuma Y: Overlap of idiopathic portal hypertension and scleroderma: report of two autopsy cases and a review of literature. J Gastroenterol Hepatol 2002, 17:217–223
11. Saito K, Nakanuma Y, Takegoshi K, Ohta G, Obata Y, Okuda K, Kameda H: Non-specific immunological abnormalities and association of autoimmune diseases in idiopathic portal hypertension. A study by questionnaire. Hepatogastroenterology 1993, 40:163–166
12. Charles C, Clements P, Furst DE: Systemic sclerosis: hypothesis-driven treatment strategies. Lancet 2006, 367:1683–1691
13. Verrecchia F, Mauviel A, Farge D: Transforming growth factor-beta signaling through the Smad proteins: role in systemic sclerosis. Autoimmun Rev 2006, 5:563–569
14. Snowden N, Coupes B, Herrick K, Illingworth K, Jayson MV, Brenchley PEC: Plasma TGF beta in systemic sclerosis: a cross-sectional study. Ann Rheum Dis 1994, 53:763–767
15. Karasek MA: Does transformation of microvascular endothelial cells into myofibroblasts play a key role in the etiology and pathology of fibrotic disease? Med Hypotheses 2007, 68:650–655
16. Chaudhuri V, Zhou L, Karasek M: Inflammatory cytokines induce the transformation of human dermal microvascular endothelial cells into myofibroblasts: a potential role in skin fibrogenesis. J Cutan Pathol 2007, 34:146–153
17. Zeisberg EM, Tarnavski O, Zeisberg M, Dorfman AL, McMullen JR, Gustafsson E, Chandraker A, Yuan X, Pu WT, Roberts AB, Neilson EG, Sayegh MH, Izumo S, Kalluri R: Endothelial-to-mesenchymal transition contributes to cardiac fibrosis. Nat Med 2007, 13:952–961
18. Zeisberg EM, Potenta S, Xie L, Zeisberg M, Kalluri R: Discovery of endothelial to mesenchymal transition as a source for carcinoma-associated fibroblasts. Cancer Res 2007, 67:10123–10128
19. Arciniegas E, Frid MG, Douglas IS, Stenmark KR: Perspectives on endothelial-to-mesenchymal transition: potential contribution to vascular remodeling in chronic pulmonary hypertension. Am J Physiol Lung Cell Mol Physiol 2007, 293:1–8
20. Liebner S, Cattelino A, Gallini R, Rudini N, Iurlaro M, Piccolo S, Dejana E: Beta-catenin is required for endothelial-mesenchymal transformation during heart cushion development in the mouse. J Cell Biol 2004, 166:359–367
21. Frid MG, Kale VA, Stenmark KR: Mature vascular endothelium can give rise to smooth muscle cells via endothelial-mesenchymal transition: in vitro analysis. Circ Res 2002, 90:1189–1196
22. Inagaki Y, Okazaki I: Emerging insights into transforming growth factor beta Smad signal in hepatic fibrogenesis. Gut 2007, 56: 284–292
23. Kinoshita K, Iimuro Y, Otogawa K, Saila S, Inagaki Y, Nakajima Y, Kawada N, Fujimoto J, Friedman SL, Ikeda K: Adenovirus-mediated

expression of BMP-7 suppresses the development of liver fibrosis in rats. Gut 2007, 56;706–714
24. Sugimoto H, Yang C, LeBleu VS, Soubasakos MA, Giraldo M, Zeisberg M, Kalluri R: BMP-7 functions as a novel hormone to facilitate liver regeneration. FASEB J 2007, 21:256–264
25. Wynn TA: Cellular and molecular mechanisms of fibrosis. J Pathol 2008, 214:199–210
26. Sato Y, Harada K, Ozaki S, Furubo S, Kizawa K, Sanzen T, Yasoshima M, Ikeda H, Sasaki M: Cholangiocytes with mesenchymal features contribute to progressive hepatic fibrosis of the polycystic kidney rat. Am J Pathol 2007, 171:1859–1871
27. Dong C, Zhu S, Wang T, Yoon W, Li Z, Alvarez RJ, Dijke PT, White B, Wingley FM, Goldschmidt-Clermont PJ: Deficient Smad expression: A putative molecular defect in scleroderma. Proc Natl Acad Sci USA 2002, 99:3908–3913
28. Nguyen LN, Furuya MH, Wofraim LA, Nguyen AP, Houdren MS, Campbell JS, Knight B, Yeoh GC, Fausto N, Parks WT: Transforming growth factor-beta differentially regulates oval cell and hepatocyte proliferation. Hepatology 2007, 45:31–41
29. Nanji AA, Tahan SR, Golding M, Khwaja S, Rahemtulla A, Laiani EN: Role of transforming growth factor-beta1 in inhibiting endothelial cell proliferation in experimental alcoholic liver disease. Am J Pathol 1996, 148:739–747
30. Okuno M, Moriwaki H, Imai S, Muto Y, Kawada N, Suzuki Y, Kojima S: Retinoids exacerbate rat liver fibrosis by inducing the activation of latent TGF-beta in liver stellate cells. Hepatology 1997, 26:913–921
31. Ramm GA, Nair VG, Bridle KR, Shepherd RW, Crawford DH: Contribution of hepatic parenchymal and nonparenchymal cells to hepatic fibrogenesis in biliary atresia. Am J Pathol 1998, 153:527–535
32. Sato Y, Sawada S, Kozaka K, Harada K, Sasaki M, Matsui O, Nakanuma Y: Significance of enhanced expression of nitric oxide syntheses in splenic sinus lining cells in altered portal hemodynamics of idiopathic portal hypertension. Dig Dis Sci 2007, 52:1987–1994
33. Akahoshi T, Hashizume M, Tanoue K, Shimabukuro R, Gotoh N, Konishi K, Tsutsumi N, Sugimachi K: Role of the spleen in liver fibrosis in rats may be mediated by transforming growth factor beta-1. J Gastroenterol Hepatol 2002, 17:59–65
34. Needleman BW, Choi J, Burrows-Menzu A, Fontana JA: Secretion and binding of transforming growth factor-b by scleroderma and normal dermal fibroblasts. Arthritis Rheum 1990, 33:650–653
35. Gabrielli A, Di Loreto C, Taborro R, Candela M, Sambo P, Nitti C, Danieli MG, DeLustro F, Dasch JR, Danieli G: Immunohistochemical localization of intracellular and extracellular associated TGF-b in the skin of patients with systemic sclerosis (scleroderma) and primary Raynaud's phenomenon. Clin Immunol Immunopathol 1993, 68: 340–349
36. Hasegawa M, Sato S, Takehara K: Augumented production of transforming growth factor-beta by cultured peripheral blood mononuclear cells from patients with systemic sclerosis. Arch Dermatol Res 2004, 296:89–93
37. Assoian RK, Komoriya A, Meyers CA, Miller DM, Sporn MB: Transforming growth factor-beta in human platelets. Identification of a major storage site, purification, and characterization. J Biol Chem 1983, 258:7155–7160
38. Oberhammer F, Bursch W, Pazefall W, Breit P, Erber E, Stadler M, Schulte-Hermann R: Effect of transforming growth factor beta on cell death of cultured rat hepatocytes. Cancer Res 1991, 51:2478–2485
39. Paradis V, Dargere D, Vidaud M, De Gouville AC, Huet S, Martinez V, Gauthier JM, Ba N, Sobesky R, Ratziu V, Bedossa P: Expression of connective tissue growth factor in experimental rat and human liver fibrosis. Hepatology 1999, 30:968–976
40. Morikawa H, Tamori A, Nishiguchi S, Enomoto M, Habu D, Kawada N, Siomi S: Expression of connective tissue growth factor in the human liver with idiopathic portal hypertension. Mol Med 2007, 13:240–245
41. Sato Y, Sawada S, Nakanuma Y: Fibulin-5 is involved in phlebosclerosis of major portal vein branches associated with elastic fiber deposition in idiopathic portal hypertension. Hepatol Res 2008, 38:166–173

Differential MicroRNA Expression Between Hepatitis B and Hepatitis C Leading Disease Progression to Hepatocellular Carcinoma

Shunsuke Ura,[1] Masao Honda,[1,2] Taro Yamashita,[1] Teruyuki Ueda,[1] Hajime Takatori,[1] Ryuhei Nishino,[1] Hajime Sunakozaka,[1] Yoshio Sakai,[1] Katsuhisa Horimoto,[3] and Shuichi Kaneko[1]

MicroRNA (miRNA) plays an important role in the pathology of various diseases, including infection and cancer. Using real-time polymerase chain reaction, we measured the expression of 188 miRNAs in liver tissues obtained from 12 patients with hepatitis B virus (HBV)-related hepatocellular carcinoma (HCC) and 14 patients with hepatitis C virus (HCV)-related HCC, including background liver tissues and normal liver tissues obtained from nine patients. Global gene expression in the same tissues was analyzed via complementary DNA microarray to examine whether the differentially expressed miRNAs could regulate their target genes. Detailed analysis of the differentially expressed miRNA revealed two types of miRNA, one associated with HBV and HCV infections (n = 19), the other with the stage of liver disease (n = 31). Pathway analysis of targeted genes using infection-associated miRNAs revealed that the pathways related to cell death, DNA damage, recombination, and signal transduction were activated in HBV-infected liver, and those related to immune response, antigen presentation, cell cycle, proteasome, and lipid metabolism were activated in HCV-infected liver. The differences in the expression of infection-associated miRNAs in the liver correlated significantly with those observed in Huh7.5 cells in which infectious HBV or HCV clones replicated. Out of the 31 miRNAs associated with disease state, 17 were down-regulated in HCC, which up-regulated cancer-associated pathways such as cell cycle, adhesion, proteolysis, transcription, and translation; 6 miRNAs were up-regulated in HCC, which down-regulated anti-tumor immune response. *Conclusion:* miRNAs are important mediators of HBV and HCV infection as well as liver disease progression, and therefore could be potential therapeutic target molecules. (HEPATOLOGY 2009;49:1098-1112.)

MicroRNA (miRNA) is an endogenous, small, single-strand, noncording RNA consisting of 20 to 25 bases and regulates gene expression of various cell types. It plays an important role in various biological processes, including organ development and differentiation as well as cellular death and proliferation, and is also involved in various diseases such as infection and cancer.[1-3]

miRNAs are produced as follows. A primary miRNA with a hairpin loop structure is cleaved into a precursor miRNA and transported out of the nuclei with a carrier protein (Exportin-5). The precursor miRNA is then processed by Dicer and converted into an active single-strand RNA in the cytoplasm. The miRNA binds to a target messenger RNA in a sequence-dependent manner and induces degradation of the target messenger RNA and translational inhibition. One miRNA regulates the expression of multiple target genes; bioinformatics analyses have suggested that the expression of more than 30% of human genes is regulated by miRNAs.[4-7]

Abbreviations: cDNA, complementary DNA; CH, chronic hepatitis; CH-B, chronic hepatitis B; CH-C, chronic hepatitis C; HBV, hepatitis B virus; HCC, hepatocellular carcinoma; HCC-B, hepatitis B-related hepatocellular carcinoma; HCC-C, hepatitis C-related hepatocellular carcinoma; HCV, hepatitis C virus; miRNA, microRNA; RTD-PCR, real-time detection polymerase chain reaction; SVM, support vector machine.

From the Departments of [1]Gastroenterology and [2]Advanced Medical Technology, Kanazawa University Graduate School of Medicine, Kanazawa, Japan; and the [3]Biological Network Team, Computational Biology Research Center, National Institute of Advanced Industrial Science and Technology, 2-42 Aomi, koto-ku, Tokyo 135-0064, Japan.

Received July 3, 2008; accepted November 15, 2008.

Address reprint requests to: Masao Honda, M.D., Ph.D., Department of Gastroenterology, Graduate School of Medicine, Kanazawa University, Takara-Machi 13-1, Kanazawa 920-8641, Japan. E-mail: mhonda@m-kanazawa.jp; fax: (81)-76-234-4250.

Copyright © 2009 by the American Association for the Study of Liver Diseases.

Published online in Wiley InterScience (www.interscience.wiley.com).

DOI 10.1002/hep.22749

Potential conflict of interest: Nothing to report.

Additional Supporting Information may be found in the online version of this article.

Table 1. Characteristics of Patients Used for Analysis of miRNA and Microarray Samples

Patient No.	Virus	Age	Sex	ALT	Histology of Activity	Background Liver Fibrosis	Histological Grade of HCC	Tumor Size (mm)	TNM Staging	HCV-RNA (KIU/mL)	HBV-DNA (LEG/mL)
1	HBV	57	M	16	2	4	Moderate	20	II	–	3.4
2	HBV	51	M	57	1	2	Moderate	48	II	–	< 2.6
3	HBV	61	M	17	1	4	Well	16	II	–	< 3.7
4	HBV	47	M	19	1	4	Moderate	15	I	–	< 3.7
5	HBV	72	M	19	1	1	Well	25	II	–	NA
6	HBV	73	M	62	1	3	Moderate	45	III	–	5.7
7	HBV	42	M	36	1	4	Moderate	18	I	–	< 3.7
8	HBV	63	M	13	1	2	Moderate	15	I	–	2.8
9	HBV	68	F	54	1	2	Well	56	II	–	4.1
10	HBV	70	M	13	0	2	Well	40	II	–	< 3.7
11	HBV	58	M	29	1	4	Moderate	35	IVA*	–	3.3
12	HBV	72	M	22	1	4	Moderate	18	I	–	6
13	HCV	66	F	33	2	4	Well	25	II	423	–
14	HCV	67	M	89	1	4	Well	30	II	> 850	–
15	HCV	64	M	31	1	4	Moderate	75	III	< 5 (+)	–
16	HCV	68	M	30	0	4	Well	23	II	> 850	–
17	HCV	46	M	98	2	3	Moderate	20	I	> 850	–
18	HCV	68	F	32	2	4	Moderate	25	III	< 5 (+)	–
19	HCV	66	F	46	2	4	Well	25	II	> 850	–
20	HCV	47	M	246	1	3	Moderate	20	I	262	–
21	HCV	75	M	27	1	3	Moderate	19	II	85.1	–
22	HCV	77	M	21	0	1	Moderate	20	II	< 5 (−)	–
23	HCV	66	M	46	2	2	Well	60	II	50.3	–
24	HCV	65	M	89	1	1	Poorly	25	III	850	–
25	HCV	53	M	54	0	1	Moderate	28	II	< 5 (−)	–
26	HCV	75	F	212	1	4	Well	19	I	580	–
27	–	51	F	18	0	0	–	–	–	–	–
28	–	78	F	13	0	0	–	–	–	–	–
29	–	75	M	20	0	0	–	–	–	–	–
30	–	34	M	12	0	0	–	–	–	–	–
31	–	64	M	30	0	0	–	–	–	–	–
32	–	78	M	9	0	0	–	–	–	–	–
33	–	53	M	19	0	0	–	–	–	–	–
34	–	64	F	12	0	0	–	–	–	–	–
35	–	60	F	20	0	0	–	–	–	–	–

HCV RNA was assayed via Amplicor Monitor Test (KIU/mL); HBV DNA was assayed via transcription-mediated amplification (LEG/mL).

Abbreviations: ALT, alanine aminotransferase; F, female; HBV, hepatitis B virus; HCC, hepatocellular carcinoma; HCV, hepatitis C virus; M, male; TNM, tumor-node–metastasis.

*Vascular invasion (+).

Infection of the human liver with hepatitis B virus (HBV) and hepatitis C virus (HCV) induces the development of chronic hepatitis (CH), cirrhosis, and in some instances hepatocellular carcinoma (HCC).[8] The virological features of these two distinct viruses are completely different; however, the viruses infect the liver and cause CH, which is not distinguished by histological examination or clinical manifestations. We previously reported that gene expression profiles in chronic hepatitis B (CH-B) and chronic hepatitis C (CH-C) are different. Proapoptotic and DNA repair responses were predominant in CH-B, and inflammatory and antiapoptotic phenotypes were predominant in CH-C. However, factors inducing these differences in gene expression remain to be elucidated.[9,10]

We examined miRNA expression in liver tissue with HBV-related liver disease (CH-B and HCC-B) and HCV-related liver disease (CH-C and HCC-C) and in normal liver tissue via real-time detection polymerase chain reaction (RTD-PCR). We also performed global analysis of messenger RNA expression in these tissues using complementary DNA (cDNA) microarray. These analyses allowed us to find characteristic miRNAs associated with HBV or HCV infection as well as the progression of liver disease.

Patients and Methods

Patients. The study subjects included 12 patients with CH-B complicated by HCC and 14 patients with

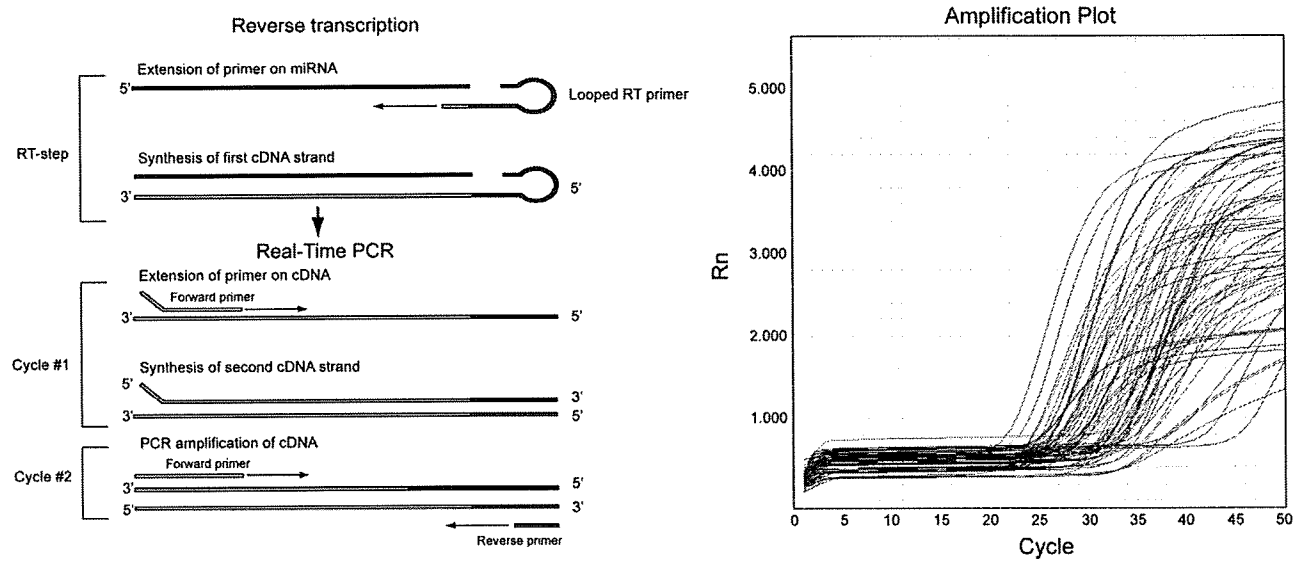

Fig. 1. (A) miRNA-specific RTD-PCR using sheet hairpin primers. (B) miRNA amplification curves by RTD-PCR.

CH-C complicated by HCC. Gene expression analysis was approved by the ethics committee of the Graduate School of Medicine, Kanazawa University Hospital, Japan, between 1999 and 2004. In addition, nine normal liver tissue samples obtained during surgery for metastatic liver cancer were used as control samples. Surgically removed liver tissues were stored in liquid nitrogen until analysis. Histological classification of HCC and histological evaluation of hepatitis in noncancerous regions for each patient are shown in Table 1. HCV viremia in two patients with CH-C was persistently cleared by interferon therapy before HCC development. There were no significant differences in the histological findings of HCC and noncancerous regions, as well as in sex, age, and hepatic function between the HBV and HCV infection groups.

Quantitative RTD-PCR. Approximately 1 mg of each liver tissue sample stored in liquid nitrogen was ground with a homogenizer while still frozen, and total RNA containing miRNA was isolated according to the protocol of the mirVana miRNA Isolation kit (Ambion, Austin, TX) and stored at −80°C until analysis. miRNA expression levels were quantitated using the TaqMan MicroRNA Assays Human Panel Early Access kit (Applied Biosystems, Foster City, CA). cDNA was prepared via reverse transcription using 10 ng each of the isolated total RNA and 3 μL each of the reverse transcription primers with specific loop structures. Reverse transcription was performed using the TaqMan MicroRNA Reverse Transcription kit (Applied Biosystems) according to the manufacturer's protocol. Then, a mixture of 6.67 μL of nuclease-free water, 10 μL of TaqMan 2 × Universal PCR Master Mix (No AmpErase UNG; Applied Biosystems), and 2 μL of TaqMan MicroRNA Assay Mix, which was included in the kit, was prepared for each sample on a 384-well plate; 1.33 μL of the reverse transcription product was added to the mixture, and amplification reaction was performed on an ABI PRISM 7900HT (Applied Biosystems). Expression levels of 188 miRNAs in each sample were quantitated.

Analysis of RTD-PCR Data. The measured 188 miRNAs included RNU6B, which is commonly used as a control for miRNA. β-Actin and glyceraldehyde 3-phosphate dehydrogenase were also measured simultaneously for correcting RNA amount. The mean Ct values and standard deviations of each miRNA were calculated from expression data of all patients obtained by RTD-PCR. miRNA with the lowest expression variation was used as the internal control. Ct values of each miRNA were then corrected by the Ct value of the internal control to yield $-\Delta$Ct values defined as relative miRNA expression levels and used for analyses. Statistical analyses and hierarchical cluster analyses of expression data were performed using BRB ArrayTools (http://linus.nci.nih.gov/BRB-ArrayTools.html). Relative miRNA expression levels were further normalized using the median over the all patients so that the normalized expression levels of each patient have a median log ratio of 0. A class prediction method was used for classifying two patient groups based on the supervised learning method, and a binary tree classification method was used for classifying three or more patient groups with a statistical algorithm of the support vector machine (SVM). Class prediction was performed using SVM incorporating genes differentially expressed at a univariate parametric significance level of $P = 0.01$. The prediction rate was estimated via cross-validation and the bootstrap method for small sample data.[11] (It is worth

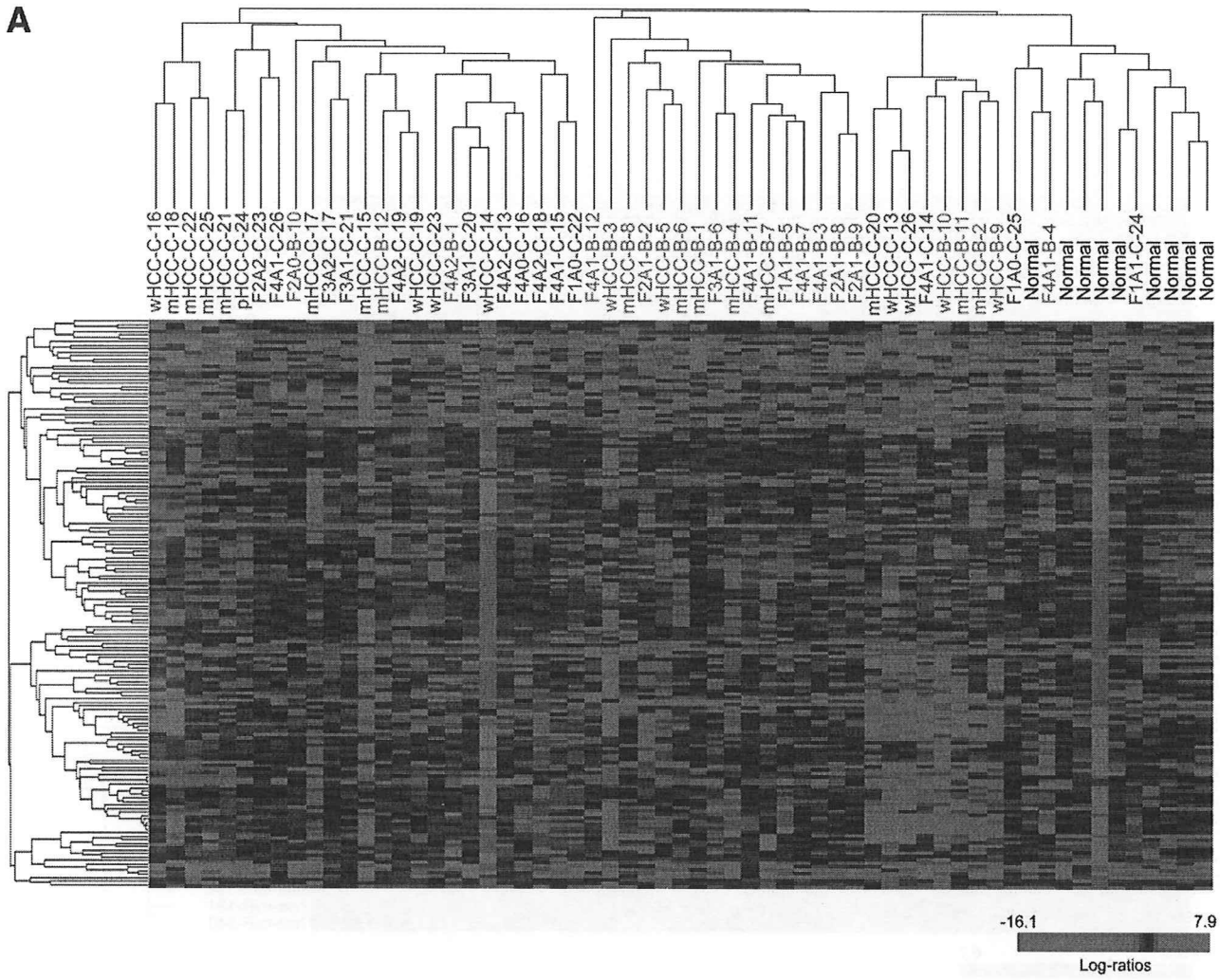

Fig. 2. (A) Hierarchical cluster analysis using total miRNA. Chronic hepatitis is indicated by histological stage and grade (F, fibrosis; A, activity) and type of infecting virus (B or C). HCC is indicated by histological grade (w, well differentiated; m, moderately differentiated; p, poorly differentiated) and type of infecting virus (B or C), with the patient number added at the end. (B) Relationship between five classes divided by binary tree classification. Expression profiles were first classified into normal liver and non-normal liver groups (node 1), then into HBV and HCV groups (node 2). The HBV group was further divided into HCC-B and CH-B (node 3), and the HCV group into HCC-C and CH-C (node 4).

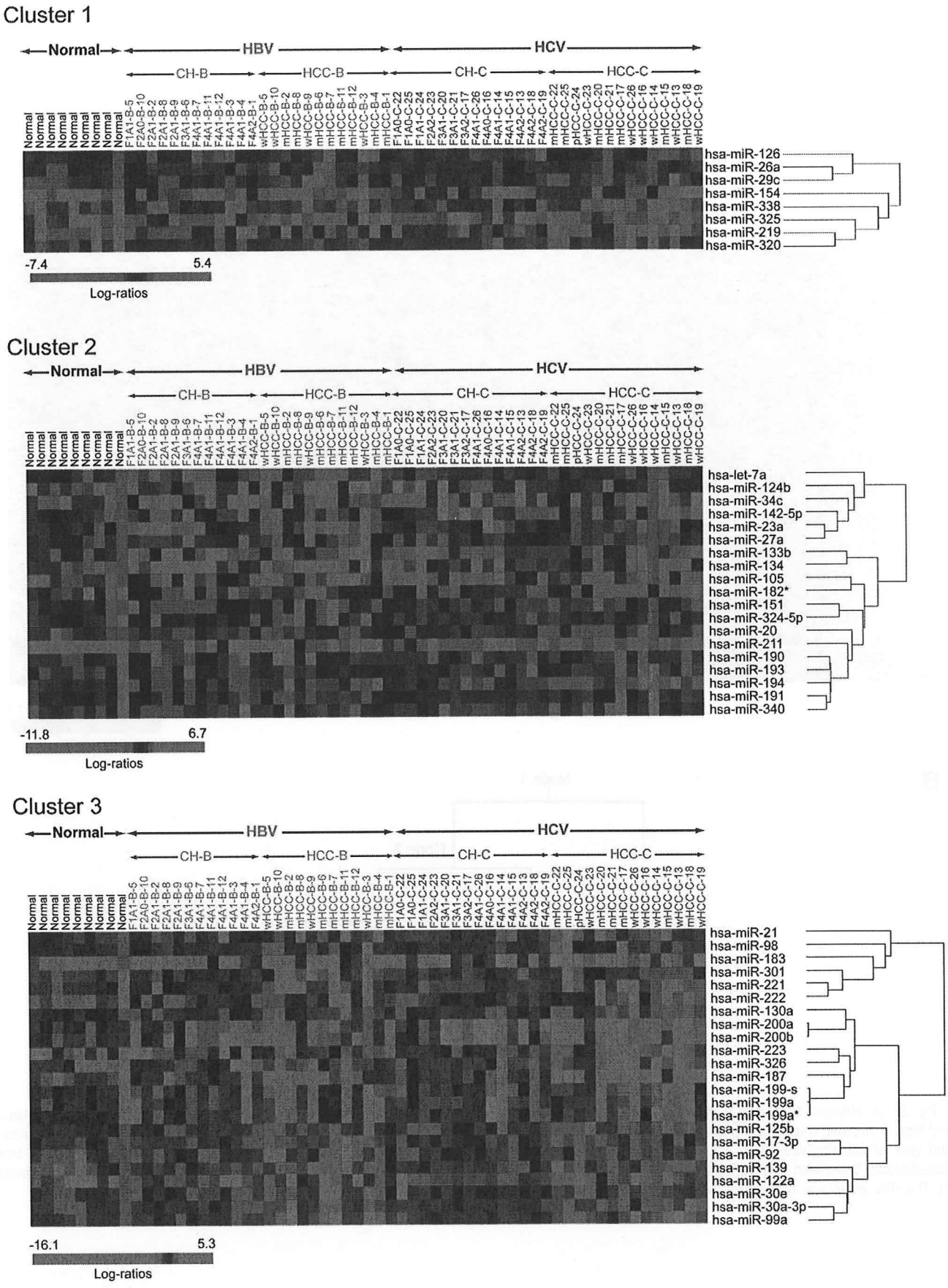

Fig. 3. Cluster 1: Eight miRNAs specifically differentiated node 1 classification. Cluster 2: Nineteen miRNAs specifically differentiated node 2 classification. Cluster 3: Twenty-three miRNAs differentiated CH-B and HCC-B as well as CH-C and HCC-C.

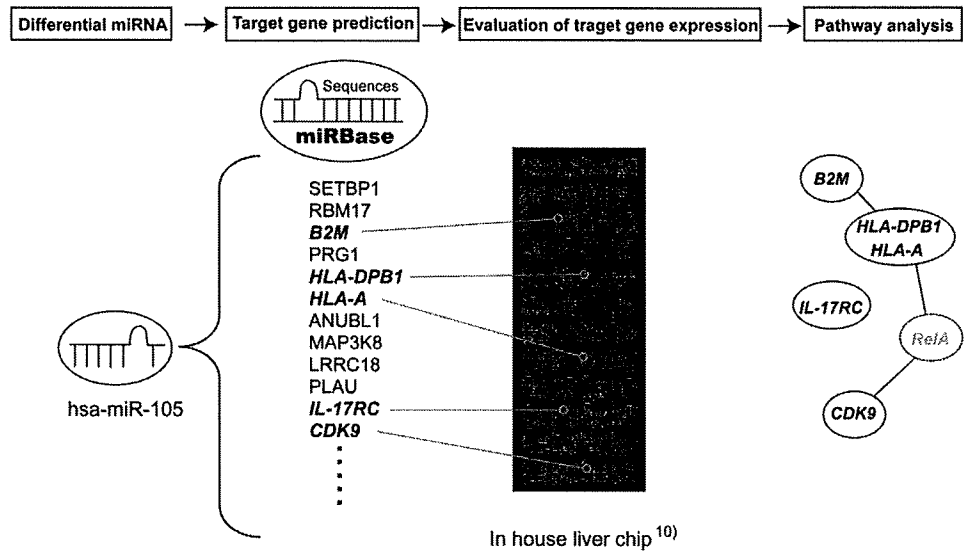

Fig. 4. Analysis of miRNA expression data. Target genes of miRNAs were predicted using MIRANDA Pro3.0; candidate target genes spotted on microarray were identified; number of genes that actually exhibit significant ($P < 0.05$) changes in expression among the genes was determined; and signal pathways involving genes regulated by the miRNAs that had exhibited differential expression between each group were analyzed using MetaCore (Table 4).

noting that the prediction rate may be likely an overestimate of the true rate, given the weaknesses of cross-validation and bootstrapping methods in a strict sense.)

Microarray Analysis. cDNA microarray slides (Liver chip 10k) were used as described.[10] RNA isolation, amplification of antisense RNA, labeling, and hybridization were performed according to the protocols described.[9,10] Quantitative assessment of the signals on the slides was performed by scanning on the ScanArray 5000 (General Scanning, Watertown, MA) followed by image analysis using GenePix Pro 4.1 (Axon Instruments, Union City, CA) as described.[10]

Preliminary Survey of Independency of Paired Samples from the Same Patient. CH and HCC expression data were derived from the same patient. Before further analysis, we examined whether the miRNA expression of paired samples was similar or independent. We compared differences in the expressions of paired and nonpaired CH and HCC samples using the Dunnett test[12] (Supplementary Data). All possible tests performed for data pairs represented no dependency due to the paired data from the same patients. For data analysis, we used the standard pairwise class comparison and prediction tool in BRB ArrayTools.

Identification of Candidate miRNA Target Genes. Candidate target genes predicted to be regulated by miRNAs based on sequence comparison were selected using MIRANDA Pro3.0 (Sanger Institute). Of the selected genes, those represented on a microarray chip were then examined for expression (Fig. 4). The number of genes showing a significant ($P < 0.05$) expression difference among the candidate target genes represented on the chip was statistically analyzed to evaluate the significance of expression regulation by miRNAs. Analysis of significance was performed using Hotelling T2 test (BRB ArrayTools).

Pathway Analysis. Of the candidate miRNA target genes, those showing a significant ($P < 0.01$) expression difference between N, CH-B, HCC-B, CH-C, and HCC-C samples were analyzed for pathways involving these genes using MetaCore software suite (GeneGo, St. Joseph, MI). Significance probability was calculated using

Table 2-1. Class Prediction

No.	Class	Prediction (%)	No. of Predictors	*P* Value
1	HBV versus HCV	87	32	<0.001
2	N versus CH (B+C)	91	26	0.007
3	CH (B+C) versus HCC (B+C)	92	34	0.003

Class prediction algorithm was used for the classification of two groups of patients. Feature selection was based on the univariate significance level (alpha = 0.01). The support vector machine classifier was used for class prediction.

Abbreviations: CH, nontumor lesion of HCC; HCC, hepatocellular carcinoma; N, normal.

Table 2-2 Binary Tree Classification

Node	Group 1 Class	Group 2 Class	No. of Predictors	Misclassification Rate (%)
1	HCC-B, HCC-C, CH-B, CH-C	N	20	4.9
2	HCC-B, CH-B	HCC-C, CH-C	19	13.5
3	HCC-B	CH-B	15	29.2
4	HCC-C	CH-C	14	17.9

Binary tree classification algorithm was used for the classification of each category of patients. Feature selection was based on the univariate significance level (alpha = 0.01). The support vector machine classifier was used for class prediction. There were four nodes in the classfication tree.

Abbreviations: CH-B, non-tumor lesion of HCC-B; CH-C, nontumor lesion of HCC-C; HCC-B, hepatitis B virus-related hepatocellular carcinoma; HCC-C, hepatitis C virus-related hepatocellular carcinoma; N, normal

Table 3-1. Representative miRNAs That Were Commonly Repressed in CH-B, CH-C, HCC-B, and HCC-C Compared with Normal Liver (Cluster)

miRNA	Parametric *P* Value	Ratio*	No. of Significant Genes/Predicted Target Genes†	Hotelling Test *P* Value‡	Differentially Expressed Target Genes§	Pathway of Regulated Genes¶
hsa-miR-219	7.3E-05	0.28	25/109	2.59E-04	Glypican-3, ERP5, PLK2, HIRA, HMG2	Regulatory T cell differentiation
					ACOX1	Fatty acid beta-oxidation
					NF-X1	MHC class II biosynthetic process
hsa-miR-320	9.8E-05	0.50	26/88	3.50E-06	Vimentin, ALP (*N*-acetyltransferase-like), SEC61 beta, G-protein alpha-i2, Filamin A	Protein kinase cascade
					Rac1, RhoG	Organelle organization and biogenesis
					Vinexin beta, Profilin I, Ca-ATPase3	Actin cytoskeleton organization and biogenesis
hsa-miR-154	2.7E-04	0.15	22/70	5.40E-06	OTR, NET1(TSPAN1), NAP1, Vimentin, PDIA3, cytochrome P-450 reductase	Regulation of apoptosis
					DLX2	Morphogenesis
					GUAC, ACAT1	Branched chain family amino acid catabolic process
hsa-miR-29c	1.8E-03	0.55	53/133	1.00E-06	FBXO7, ASPP1, HSPA4, Cathepsin O, PDF, COL4A1, HSPA4, TIP30, CXADR	Cell-substrate adhesion
					NS1-BP, ALP (*N*-acetyltransferase-like), ACTR10, Beclin 1	Transcription, DNA-dependent
					SMAD6, LTBR(TNFRSF3), ENPP7	Apoptosis
hsa-miR-338	5.2E-03	0.46	30/101	3.60E-06	ID3, GATA-4, NFIA, FR-beta, CREST, HYOU1	Developmental process
					G3ST1, CAD,	Immune effector process
					FKBP12, LZIP, PDIA3, Schwannomin (NF2), CREST	Immune system process
hsa-miR-26a	6.3E-03	0.70	37/119	2.64E-05	*LIG4*, c-FLIP, GADD45 beta, DAPK1, PRDX4, LRP130	Response to stimulus
					Cyclin E, ZDHHC6, Tx1, ATG8 (GATE-16), WASP, C1s	DNA replication initiation
					COPG1	Ion transport
hsa-miR-126	8.1E-03	0.65	27/101	4.04E-03	ANP32B (april), HSPA4, RLI, LIV-1 (SLC39A6), PTP-MEG2, CD97, DHPR	Regulation of cellular protein metabolic process
					NFKBIA, NMI, MDH1, PDCD2	Response to stress
					SMAD6, ATP6AP2, ANP32B (april), NMI, HSPA4	Apoptosis
hsa-miR-325	8.7E-03	0.20	18/63	2.03E-04	TRADD, CREST, NEDD8, annexin IV, GPX2, PDF, TNFAIP1	Developmental process
					Glypican-3, ID1, PC-TP,	Multicellular organismal development
					SNRPB (Sm-B)	RNA splicing

*Ratio of HCC-B, HCC-C, CH-B, and CH-C to normal.
†The number of significant genes ($P < 0.05$) out of predicted target genes in which expression was evaluated in microarray.
‡Statistical assessment of presence of differentially expressed genes out of predicted target genes of miRNAs.
§Representative differentially expressed genes out of predicted target genes of miRNAs.
¶Representative pathway of differentially expressed genes out of predicted target genes of miRNAs.

the hypergeometrical distribution based on gene ontology terms. Because one gene is frequently involved in multiple pathways, all pathways corresponding to the genes with significance probability were listed.

Verification of Regulation of Candidate Target Genes by miRNAs. Anti-miRNA (Ambion) specific to 13 miRNAs (has-miR-17*, has-miR-20a, has-miR-23a, has-miR-26a, has-miR-27a, has-miR-29c, has-miR-30a, has-miR-92, has-miR-126, has-miR-139, has-miR-187, has-miR-200a, and has-miR-223) showing significant differences in expression were transfected into Huh7 cells using TransMessenger transfection reagent (QIAGEN, Valencia, CA), and loss of function of each miRNA was evaluated. Similarly, precursor miRNAs of five miRNAs (has-miR-23a, has-miR-26a, has-miR-27a, has-miR-92, and has-miR-200a) were also transfected into Huh7 cells, and gain of function of each miRNA was evaluated. The loss- and gain-of-function of miRNAs were evaluated via RTD-PCR. In addition, different gene expressions regulated by miRNAs were also evaluated via RTD-PCR.